Available online at www.sciencedirect.com
SCIENCE DIRECT®
Coordination Chemistry Reviews 248 (2004) 1195–1213
COORDINATION CHEMISTRY REVIEWS
www.elsevier.com/locate/ccr

Review

Kinetics and mechanism of electron injection and charge recombination in dye-sensitized nanocrystalline semiconductors

Ryuzi Katoh [a], Akihiro Furube [a], Alexander V. Barzykin [a], Hironori Arakawa [a], M. Tachiya [b,*]

[a] *Photoreaction Control Research Center (PCRC), National Institute of Advanced Industrial Science and Technology (AIST), AIST-Central, Tsukuba, Ibaraki 305-8565 Japan*
[b] *National Institute of Advanced Industrial Science and Technology (AIST), AIST-Central, Tsukuba, Ibaraki 305-8565 Japan*

Received 15 October 2003; accepted 9 March 2004
Available online 19 May 2004

Contents

Abstract

Our recent experimental and theoretical work on the kinetics and mechanism of electron injection and charge recombination in dye-sensitized nanocrystalline semiconductors is reviewed. In our experimental studies of electron injection, nanocrystalline ZnO films were chosen as the semiconductor. In order to reveal the kinetics and mechanism of electron injection we have developed several types of transient absorption spectrometers which enable us to observe the time profiles of the absorption spectra of the oxidized form of dyes and conducting electrons with high sensitivity over a wavelength range from near IR to visible and over a time range from femtoseconds to submicroseconds. For N3 dye/ZnO system, the aggregation of N3 dyes and its effect on electron injection have been clarified spectroscopically. The electron injection process has been measured by a femtosecond pump-probe method and it has been found that a fraction of electron injection occurs via an intermediate state. The absolute efficiency of electron injection has been measured and a new theoretical model has been developed for

* Corresponding author. Tel.: +81-29-861-4412; fax: +81-29-861-6201.
E-mail address: m.tachiya@aist.go.jp (M. Tachiya).

doi:10.1016/j.ccr.2004.03.017

electron injection to explain the dependence of the efficiency of electron injection on the free energy change for injection. Concerning charge recombination a consistent theoretical model has been developed which explains not only the observed highly dispersive kinetics of charge recombination but also the effects of the light intensity, the applied bias and the dye structure on the kinetics.

Keywords: Dye-sensitized solar cells; Electron injection; Charge recombination; Transient spectroscopy; Electron transfer theory; Multiple trapping model

1. Introduction

Grätzel and coworkers developed a highly efficient dye-sensitized solar cell (Grätzel cell) consisting of N3 dye (*cis*-bis-(4,4′-dicarboxy-2,2′-bipyridine)dithiocyanato ruthenium(II); $Ru(dcbpy)_2(NCS)_2$) adsorbed on nanocrystalline TiO_2 films. The solar-energy-to-electricity conversion efficiency of this cell amounts to $\eta = 10\%$ under AM 1.5 irradiation [1]. In the last decade considerable efforts have been made to improve the performance of dye-sensitized solar cells, but without much success. The detailed operating mechanism of these solar cells has been studied extensively to identify the processes that limit their performance. However, the mechanism is not fully understood, as there are still some unknown parameters that control the performance of this type of solar cell.

Fig. 1 illustrates the primary processes in dye-sensitized solar cells. Upon photoexcitation of the sensitizer dye, the electrons are injected from the excited sensitizer dyes into the conduction band (CB) of the semiconductor film (electron injection). The injected electrons recombine with the oxidized sensitizer dyes (recombination). This recombination process competes with the regeneration of the oxidized sensitizer dyes by the redox mediator molecules (rereduction). The electrons can be transported in the semiconductor film as the conducting electrons. The conducting electrons can react with the redox mediator molecules or with molecules in the solution during transport, before reaching the back contact electrode (leak reaction). Finally, the remaining electrons flow into the external circuit.

A nanocrystalline TiO_2 film is considered to be the most promising material for the electrode of dye-sensitized solar cells to realize high solar cell performance. A nanocrystalline ZnO film has also been studied as the semicondcutor electrode for the dye-sensitized solar cells because the energy level of its conduction band (−0.2 V versus NHE at pH = 1) is similar to that of TiO_2 (−0.28 V versus NHE at pH = 2) [2]. However, the performance of solar cells based on N3-adsorbed nanocrystalline ZnO film (abbreviated as N3/ZnO) is significantly lower than that of TiO_2 solar cells [3–5]. On the other hand, the solar cell performance of nanocrystalline ZnO system using organic dyes (eosin Y [6], mercurochrome [7], and so on) as sensitizer molecules is similar to that of TiO_2 system. Thus, we believe that a nanocrystalline ZnO film is a promising material for high performance solar cells.

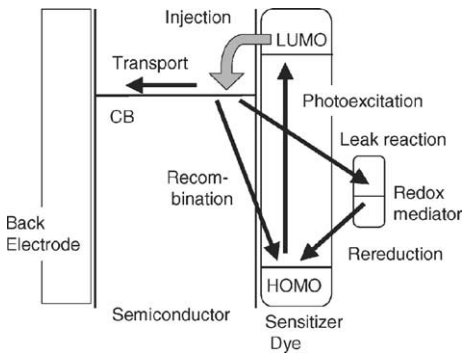

Fig. 1. Primary reaction steps in dye-sensitized solar cells.

In this paper, we review our recent work on the kinetics and mechanism of electron injection and charge recombination in dye-sensitized nanocrystalline semiconductors. In our experiment studies of electron injection, we chose ZnO as the semiconductor and have been studying electron injection processes in ZnO systems with the perspective described above [8–11]. Our work on electron injection is presented in Section 2. Charge recombination is a loss process in dye-sensitized solar cells. The kinetics and mechanism of charge recombination have been studied extensively for the purpose of improving the performance of solar cells. We have developed a consistent theoretical model to explain the observed highly dispersive kinetics of charge recombination and the effects of the light intensity, the applied bias and the dye structure on the kinetics. Our work on charge recombination is presented in Section 3.

2. Electron injection

The electron injection process is one of the most important primary processes in dye-sensitized solar cells. In this section, we present our recent results on electron injection process in ZnO system. For N3/ZnO, aggregates are formed during the preparation of sample specimen. We studied the aggregates through fluorescence spectroscopy in detail (Section 2.1). The injection process can be studied by observing absorption due to the oxidized form of sensitizer dyes or conducting electrons by transient absorption spectroscopy. The spectrum of the conducting electron appears in the near-IR wavelength range, so we have to measure the spectrum from the visible to near-IR wavelength range. The intensity and temporal profile of transient absorption signal is very sensitive to the exciting light intensity. In order to clarify the mechanism of primary processes in dye-sensitized solar cells we have to measure the transient

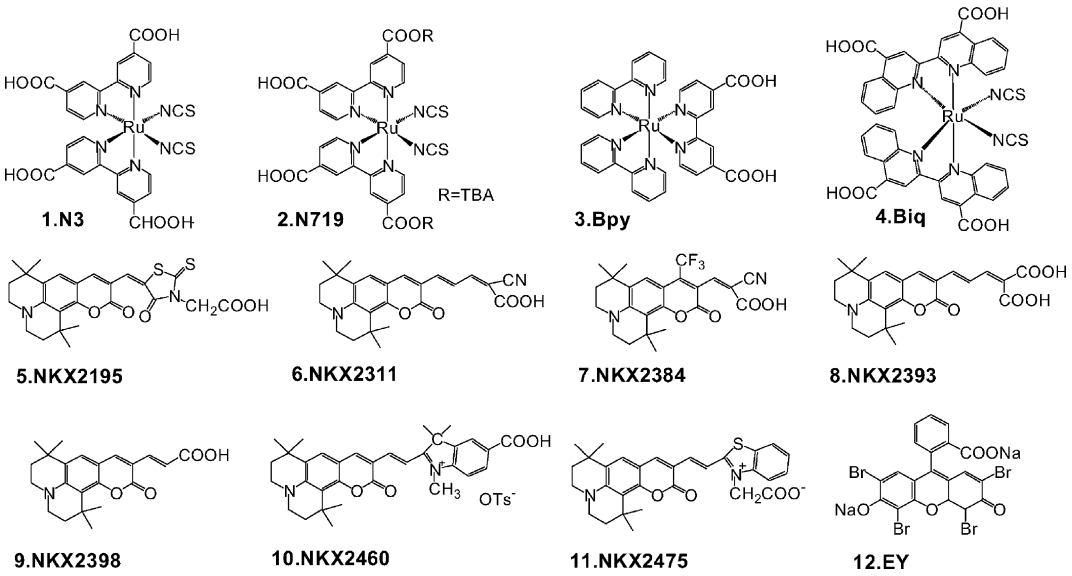

Fig. 2. Molecular structure of sensitizing molecules studied.

absorption signal at very low excitation intensities, so that a highly sensitive transient absorption spectrometer has to be developed (Section 2.2). The rate of electron injection in such a system can be determined through femtosecond transient absorption (Section 2.3). The rate of electron injection is much faster than that of fluorescence decay of sensitizer dye. Therefore, a high efficiency of electron injection can be expected. To evaluate the absolute value of the efficiency directly, nanosecond transient absorption measurement has been carried out precisely (Section 2.4.1). For N3/ZnO systems, we observed that fast injection kinetics does not lead to high efficiency (Section 2.4.3). In order to clarify the mechanism of solar cells, we measured the efficiency as a function of the free energy change for injection and proposed a new theoretical model for the electron injection process.

2.1. Sample preparation

2.1.1. Preparation procedure

A ZnO paste composed of ZnO nanoparticles (Sumitomo Osaka Cement, #100), polyvinyl acetal (Sekisui Kasei, BM-2), and α-terpineol was painted on a glass plate with a screen printer (Mitani Electronics Co., MEC-2400). Nanocrystalline films were prepared by calcination of the painted substrate for 1 h at 420 °C. The thickness of the films was about 5 μm and the films were optically transparent. The apparent area of the ZnO films was about 1 cm^2 (1 cm × 1 cm). Fig. 2 shows the molecular structures of sensitizer molecules studied. Detailed synthetic procedure of coumarin dyes has been reported elsewhere [12]. The sensitizer dyes were dissolved in dehydrated ethanol (Wako Chemicals) or *tert*-butylalcohol (Kanto, G grade)–acetonitrile (Kanto, dehydrated) mixture solvent (50:50). These solvents were used without further purification. The sample specimens were prepared by immersing the ZnO substrate into the dye solutions. The sample specimens dried in air were used for transient absorption measurements. All measurements were carried out just after preparation of the sample specimens to minimize the effect of dye degradation.

2.1.2. Formation of (N3-Zn^{2+}) aggregate on ZnO surface

To fix sensitizer dyes on ZnO surface, ZnO films are immersed into the solution of sensitizer dyes. During the process, a small amount of Zn^{2+} ion is dissolved into the solution from the surface of the ZnO films and subsequently Zn^{2+} ions attach to carboxyl groups of the sensitizer dyes (aggregate formation). This type of aggregate was reported for several organic sensitizer dyes [13,14] as well as ruthenium complexes [15]. For N3/ZnO, the IPCE (incident photon-to-current conversion efficiency) dramatically decreases with increasing immersion time of ZnO substrates in N3 dye solution [15], suggesting that primary process may be affected by the aggregation. Thus, we studied the formation of the aggregate (N3-Zn^{2+}) between N3 dye and Zn^{2+} on the nanocrystalline ZnO film in detail [10].

Fig. 3 shows the fluorescence spectra of N3 in basic (0.1 mol dm^{-3} NaOH) and acidic (0.1 mol dm^{-3} HCl) aqueous solutions. The fluorescence peaks are observed at 740 and 790 nm in basic and acidic solutions, respectively. The blue shift with increasing pH is due to the deprotonation of the carboxyl groups of N3 [16], suggesting that the fluorescence peak position of N3 is sensitive to the type of an ion attached to carboxyl groups. Fig. 3 also shows the fluorescence spectrum of a synthesized (N3-Zn^{2+}) film, which was prepared by a reported procedure [15] and was cast on a glass plate to make a film. The peak observed at 730 nm is slightly blue-shifted from that of N3 in the basic solution (740 nm). This shift reflects the structure of the aggregate (N3-Zn^{2+}), namely, N3 molecules are associated with

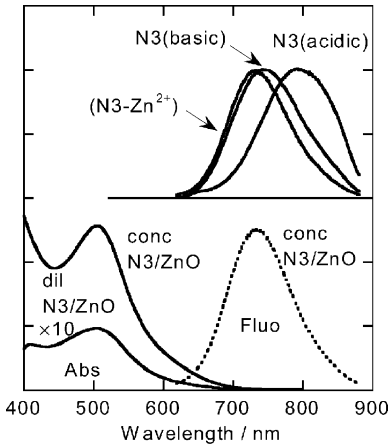

Fig. 3. Emission spectra of synthesized (N3-Zn^{2+}), and N3 in aqueous acidic (0.1 mol dm^{-3} HCl) and basic (0.1 mol dm^{-3} NaOH) solutions. Absorption spectra of dil. and conc. N3/ZnO films and emission spectrum of conc. N3/ZnO. The emission of dil. N3/ZnO film cannot be observed.

each other through carboxyl groups by sharing Zn^{2+} ion. The fluorescence peak of (N3-Zn^{2+}) can be distinguished from those of N3 in basic and acidic solutions. Therefore, the formation of (N3-Zn^{2+}) on the surface of ZnO film can be probed by observing its fluorescence spectrum.

We prepared two sample specimens with different immersion times; 3 min (dilute N3/ZnO) and 12 h (concentrated N3/ZnO). Fig. 3 shows the absorption spectra of conc. and dil. N3/ZnO films. The spectra are similar to each other, although the absorbance of conc. N3/ZnO film is 20 times as large as that of dil. N3/ZnO. In order to identify the formation of (N3-Zn^{2+}) on the surface of ZnO film, the fluorescence from N3/ZnO specimens was measured and is shown in Fig. 3. For dil. N3/ZnO, no emission was observed with our apparatus. This indicates that the excited N3 is efficiently quenched by the electron injection to the ZnO films. On the other hand, fluorescence was observed for conc. N3/ZnO with a peak at 730 nm, which is identical to that of synthesized (N3-Zn^{2+}) films. This clearly shows that (N3-Zn^{2+}) is formed on conc. N3/ZnO films, while the formation is negligible on dil. N3/ZnO films.

As we mentioned above, the formation of (N3-Zn^{2+}) can be confirmed by observing its fluorescence. The microscopic image of the fluorescence directly shows the spatial distribution of (N3-Zn^{2+}) in the sample specimen. Many bright points can be seen in the image [10]. They clearly show that micrometer-sized crystals of (N3-Zn^{2+}) are formed on the surface.

2.2. Transient absorption spectrometer

Transient absorption measurements of these systems were carried out mainly by observing the bleaching of the ground state absorption of sensitizer dyes and the absorption due to excited and oxidized sensitizer dyes in the visible wavelength range (400–900 nm). These signals often overlap with each other. Therefore, the analysis of the spectra and decay profiles is not always easy [17]. Moreover, the assignment of the absorption band of newly synthesized sensitizer dyes is usually difficult. The observation of electrons injected into the semiconductor film is more appropriate for detailed analysis, because in near-IR wavelength range the absorption due to conducting electrons in semiconductor film is expected to appear without any overlapping with other absorption bands. The absorption due to injected electrons in IR wavelength range has been observed to study dynamics of the electron injection process [11,17–20] and the loss process of conducting electrons [21,22]. It is reported that the rate of the charge recombination in nanocrystalline films is very sensitive to excitation intensity I_{ex} [9,23,24]. We have developed highly sensitive transient absorption spectrometer with wide observation wavelength range (400–3000 nm).

2.2.1. Femtosecond transient absorption spectrometer

The light source for femtosecond pump-probe transient absorption measurements is a regenerative/multipath double stage amplifier system of a Ti:sapphire laser (800 nm wavelength, 50 fs FWHM pulse width, 1.4 mJ per pulse intensity, 1 kHz repetition, Spectra Physics, Super Spitfire) combined with two optical parametric amplifiers (Spectra Physics, OPA-800). For a pump pulse the OPA output at 540 nm with intensity of several μJ per pulse was used, and for a probe pulse the OPA output or white-light continuum generated by focusing the fundamental beam into a sapphire plate was used. The probe beam transmitted through the film sample was detected by a Si, InGaAs, or MCT photodetector after passing through a monochromator (Acton Research, Spectra Pro 150). Using this apparatus, we can observe small absorbance change ($<10^{-3}$) with wide wavelength range (400–2500 nm). The detail on the apparatus is described elsewhere [11].

2.2.2. Nanosecond transient absorption spectrometer

For nanosecond transient absorption measurements, the second harmonic pulse (532 nm) from a Nd^{3+}:YAG laser (Continuum, Surelite II) was used for pumping light. The duration of the laser pulse was 8 ns. A Xe flash lamp (Hamamatsu, L4642, 2 μs pulse duration) was used as a probe light source. The probe light was focused on a sample specimen (2 mm in diameter). The area probed with the probe light was covered by that irradiated with the exciting light (5 mm in diameter). The probe light transmitted through the sample specimen was detected after being dispersed with a 10 cm monochromator, with a Si-photodiode (Hamamatsu, S-1722) in the range of 550–950 nm, with an InGaAs-photodiode (Hamamatsu, G3476-05) for 900–1600 nm range and with an MCT-photodetector (Dorotek, PDI-2TE-4) for 1200–2800 nm range. Signals from the photodetector were processed with a digital oscilloscope (Tektronix, TDS680C) and were analyzed with a computer. Small absorbance change ($<10^{-3}$) can be detected using this spectrometer.

2.2.3. Sub-microsecond transient absorption spectrometer

For a sub-microsecond transient absorption spectrometer, a Nd^{3+}:YAG laser (HOYA Continuum, Surelite II) was used for the pumping light source. The repetition rate of the laser was 10 Hz. The second harmonic pulse (532 nm) were used for the excitation of a dye-sensitized ZnO films. A halogen lamp (100 W) was used as the probe light source. The probe light was incident at 45° on the sample specimen. The transmitted light was detected with a Si-photodiode (Hamamatsu, S-1722) in the range of 550–950 nm and with an MCT-photodetector (Dorotek, PDI-2TE-4) for 950–2800 nm after being dispersed with a monochromator (ACTON, SpectraPro-150). The photocurrent from the detector was amplified with an ac-coupled pre-amplifier (NF Electronic Instruments, SA-230F5) and a differential amplifier (NF Electronic Instruments, 5305). Signals were processed with a digital oscilloscope (Tektronix, TDS380) and analyzed with a computer. Using the pre-amplifier, the dc offset of the photocurrent from the detector can be subtracted and therefore a small absorbance change ($<10^{-5}$) can be detected. The time resolution of the system was about 50 ns. To calculate the absorbance change, the value of the intensity of the probe light without laser excitation is required. It was measured by modulating the probe light intensity with an optical chopper placed in front of the detector.

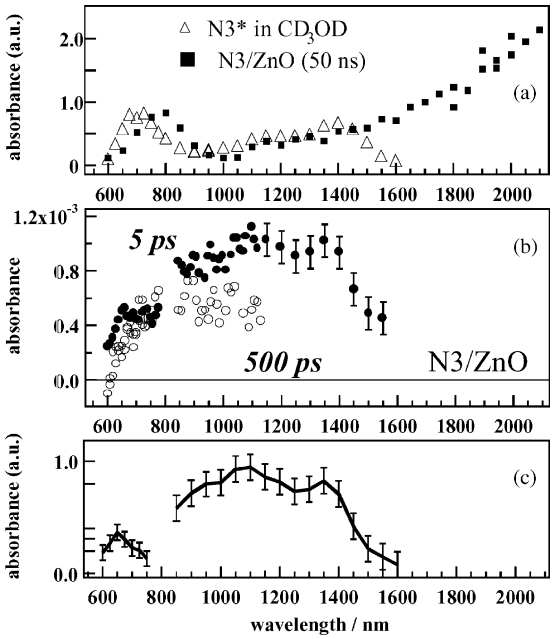

Fig. 4. (a) Transient absorption spectrum of N3 dye in deuterated methanol solution at ~10 ns delay time and N3/ZnO (nanocrystalline ZnO film absorbed with N3 dye) at 50 ns delay time. (b) Transient absorption spectra of N3/ZnO at 5 ps (closed circle) and 500 ps (open circle) delay times after excitation. (c) The spectrum of the intermediate corresponding to an exciplex.

2.3. Kinetics and mechanism of electron injection

To study the kinetics and mechanism of photo-induced ultrafast electron injection occurring from adsorbed dye into nanocrystalline semiconductor film, we have focused our attention mainly on the near-IR range for femtosecond transient absorption measurements. The dye and semiconductor investigated here are N3 and ZnO. In the near-IR range, absorption bands due to intermolecular interactions such as charge transfer and charge resonance are expected [25,26]. Strong interaction between adsorbed dye in the excited states and electron acceptor states in the semiconductor is considered to give optical transitions in the near-IR region. This kind of spectral information is useful to clarify electron injection mechanism.

Here, we present our recent results on the first observation of a near-IR absorption band during an electron injection reaction. This band appeared rapidly after the excitation of N3 dye and its disappearance is accompanied by a rise of an absorption band due to conducting electrons. From the spectral feature we assigned this intermediate state to charge transfer complex between the excited N3 dye and surface states of ZnO.

In order to analyze the dynamics of the electron injection process in N3/ZnO, we need information on the spectra of $N3^*$ (excited N3) and $N3^+$(oxidized N3). We measured the transient absorption spectrum of N3 up to 1600 nm in deuterated methanol solution using the nanosecond laser system, where the delay time was set to be just after excitation of a 8 ns pulse duration. The spectrum obtained is shown in Fig. 4a. In addition to the reported absorption peak at 700 nm, another absorption peak was observed at 1400 nm in the near-IR region for the spectrum of $N3^*$. The transient absorption spectrum for N3/ZnO at 50 ns after excitation was also measured using the nanosecond laser system, and is shown in Fig. 4a. The observed peak at 800 nm is ascribed to $N3^+$ from the similarity to the spectrum reported previously [27]. In the longer wavelength region, an absorption band whose intensity increases with wavelength is observed. This band can be assigned to the transition of free electrons in the conduction band including those from shallowly trapped electrons to higher states in the same band [28].

The transient absorption spectra at delay times of 5 and 500 ps for N3/ZnO are shown in Fig. 4b. It is seen that the absorption band at 5 ps is quite broad and seems to have a maximum at around 1200 nm (between 1000 and 1400 nm). This absorption band is quite different from that of $N3^*$, $N3^+$, or free electrons shown in Fig. 4a and b. It is obvious that even a superposition of these bands cannot reproduce this near-IR broad band, if one notices that the near-IR band has a large intensity at 1000 nm, whereas the absorbance intensities of $N3^*$, $N3^+$, and free electrons are relatively weak at this wavelength. Our result is also very different from that on $N3/TiO_2$. For the latter case only a very peak absorption due to $N3^*$ (triplet state of N3) has been reported in the wavelength region from 900 to 1100 nm by Benkö et al., and its decay with a time constant of 50 ps was ascribed to a minor component of electron injection from $N3^*$ to TiO_2 [29].

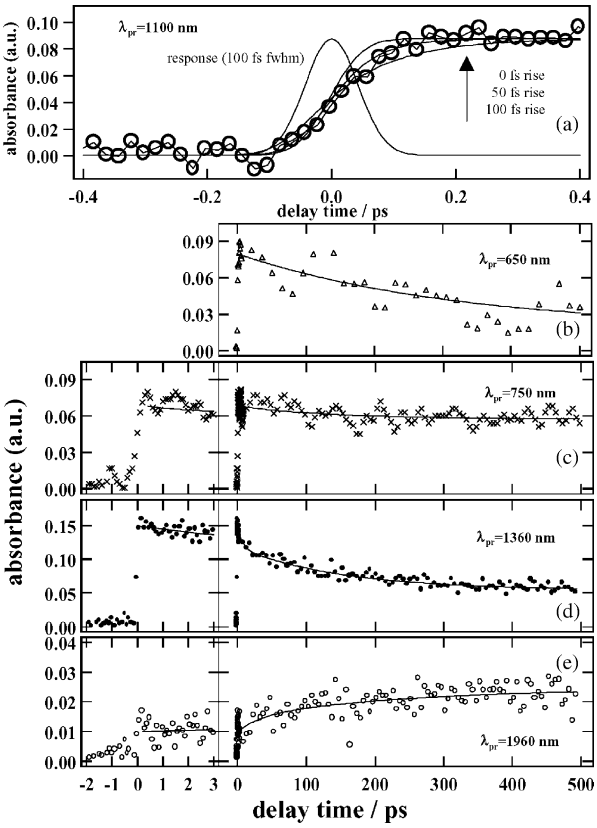

Fig. 5. Transient absorption temporal profiles of N3/ZnO at: (a) 1100 nm, along with calculated curves obtained by convoluting the response function (dashed line, 100 fs FWHM Gaussian) with the exponential rise function having rise times of 0, 50, or 100 fs. Transient absorption temporal profiles of N3/ZnO at: (b) 650, (c) 750, (d) 1360, and (e) 1960 nm.

The build up of the broad absorption was examined by measuring the time profile at the wavelength of 1100 nm in the delay time range from −0.4 to 0.4 ps. At this wavelength the contribution by N3*, $N3^+$, or free electrons would be small. Fig. 5a shows the transient absorption profile at 1100 nm and the calculated rise curves obtained by convoluting the typical response function of the apparatus (100 fs FWHM gaussian) with an exponential rise functions having 0, 50, or 100 fs rise time. It is seen that the absorption rise time is within 100 fs. Since the excitation in this experiment corresponds to the MLCT transition of N3 dye, N3* in the singlet state should be generated initially. The intersystem crossing is known to be very fast. In the case of similar Ru-complex, $[Ru(bpy)_3]^{2+}$, the time constant of intersystem crossing is reported as 40 ± 15 fs [30]. We could not observe any indication of N3* even in the triplet state although we probed at 700 or near 1400 nm around a delay time of zero ps, at which the triplet N3* has characteristic maxima. This suggests that the lifetime of N3* on ZnO is extremely short, and probably shorter than or comparable to the intersystem crossing time. At present, we cannot resolve the dynamics within 100 fs. However, an important fact is that the species giving the broad absorption band in the near-IR is produced after rapid relaxation of the MLCT excited state of N3 dye, and not by direct photoexcitation, since we excited the MLCT band of N3.

In the following, the picosecond dynamics of N3/ZnO is discussed. Panels (b)–(e) of Fig. 5, show the temporal profiles of the transient absorption of N3/ZnO probed at 650, 750, 1360, and 1960 nm, respectively. They are presented in two time ranges up to 3 and 500 ps for a clearer view. In the visible region, a slow decay is seen at 650 nm, while the absorbance is almost constant at 750 nm. The observed absorbance rise at 750 nm is as fast as the instrument response (∼150 fs for the white-light continuum probe in the visible region). Fig. 5d shows the temporal profile probed at 1360 nm. The decay could not be analyzed with a single exponential function, so that we used a biexponential function with a constant component added. Two decay constants of 6.7 ± 2.5 and 150 ± 20 ps were obtained with relative amplitudes of 17 and 43%, respectively. When the probe wavelength was shifted to longer than 1700 nm, a slow absorption rise was observed as shown in Fig. 5e. Here, the probe light was set at 1960 nm. From the result of our nanosecond experiment mentioned before, the absorption at 1960 nm is ascribed to the tail of the absorption band of free electrons, namely, conductive electrons. The rise seems to correspond to the decay at 1360 nm. The solid line in Fig. 5d is a biexponential function with a constant component added, where the two rise constants of 6.7 and 150 ps with relative amplitudes of 5 and 47%, respectively, are assumed. This rise curve is similar to the observation by Asbury et al. [18,19] using 5 μm mid-IR probe.

The near-IR band around 1200 nm is considered as an intermediate state in the course of electron transfer from N3* to the conduction band of ZnO. Considering that the intermediate has an absorption band with a maximum and is generated very rapidly after photoexcitation of N3 absorbed on the ZnO surface, and that it decays slowly to generate conductive electrons in the ZnO bulk, its origin is likely to be localized states at the surface of ZnO. The electron injection process in N3/ZnO proceeds stepwise via the intermediate states at the surface as:

$$\mathrm{N3}\overset{h\nu}{+}\mathrm{ZnO} \xrightarrow{<100\ \mathrm{fs}} \mathrm{N3^*} + \mathrm{ZnO} \xrightarrow{\sim 150\ \mathrm{ps}} \text{intermediate} \rightarrow \mathrm{N3^+} + {e_{CB}}^- \quad (1)$$

where ${e_{CB}}^-$ indicates a conducting electron in ZnO.

Since almost a half of ${e_{CB}}^-$ seems to be generated already at a few ps delay time (see Fig. 5e), the spectrum of N3/ZnO at 5 ps should include contribution of $N3^+$ and ${e_{CB}}^-$ to some extent. We have eliminated this contribution from the spectrum by a procedure described [11], in order to obtain the spectrum of the intermediate itself. The spectrum is shown in Fig. 4c.

At present, we do not know the exact nature of the intermediate. One of the possibilities of such states is simply a pair of $N3^+$ and a trapped electron at some kind of surface state. If this is the case, we should observe the $N3^+$ component as well in the spectrum of the intermediate in Fig. 4c.

However, no peak was found around 800 nm. It seems that we should rather think of more complex electronic states for the intermediate.

As another and more likely possibility for the origin of the intermediate, we propose that the excited state of N3 and the surface state of ZnO form some kind of exciplex. The former behaves as an electron donor (D^*) and the latter as an acceptor (A). The D^*A (neutral pair) and D^+A^- (ion pair) states are electronically mixed to form the exciplex states. If the D^+A^- state is lower in energy than the D^*A state, the lower and higher exciplex states have ionic and neutral character, respectively. In this case, the observed species is an ionic exciplex, and the absorption band observed in the near-IR is considered as a CT band corresponding to an ionic-to-neutral transition that transfers an electron back to N3 dye. If the D^*A state is lower in energy than the D^+A^- state, observed species is a neutral exciplex. From the spectral feature one can judge whether the observed exciplex is neutral or ionic. Generally, an ionic exciplex shows spectral features of D^+ and A^- in addition to the CT band, while a neutral one shows that of D^* in addition to the CT band. Since the observed spectrum has a shoulder at 650 nm which is relatively close to the peak of N3* at 700 nm, the whole spectrum can be understood as a superposition of the band of N3* and a CT band around 1000 nm.

It is also possible to regard the spectrum of the intermediate as an ionic exciplex, if we understand it as a superposition of a broadened $N3^+$ band and a wide CT band spread up to 1600 nm. The shoulder at 650 nm might be an artifact coming from the subtraction procedure of the intrinsic $N3^+$ band from the broadened $N3^+$ band. At present, it is difficult to assign whether the exciplex is ionic or neutral. More recently Lian and co-workers [20] reported that the vibrational spectrum of the transient species observed at the 10 ps delay time after excitation of a N3/ZnO film was attributed to the excited state of the N3 dye. Their rise dynamics of electron absorption at ~4700 nm is similar to ours at 1960 nm. Therefore, the exciplex is considered to have a neutral character, if our observation and theirs are combined.

In both cases of ionic and neutral exciplexes, we can consider the ultrafast (<100 fs) rise of the near-IR band as due to partial electron transfer from N3* to ZnO surface states to generate a $D^{\delta+}A^{\delta-}$ state ($0 < \delta < 1$). The exciplex formation within 100 fs and the resulting energy stabilization leads to the retardation of the subsequent electron injection into the bulk conduction band. This would be a reason for the slow generation of free electrons in the conduction band of ZnO. Multi-exponential decay of the near-IR band is considered to reflect the inhomogeneous distribution of the charge transfer interaction. If we take into account the exciplex formation and its dissociation described above, Scheme 1 will be modified as:

$$\mathrm{N3} \xrightarrow{h\nu} \mathrm{N3^*} + \mathrm{ZnO} \xrightarrow{<100\ \mathrm{fs}} \mathrm{N3^*} + \mathrm{ZnO} \xrightarrow{\sim 150\ \mathrm{ps}} (\mathrm{N3^*} \cdots \mathrm{ZnO}) \rightarrow \mathrm{N3^+} + \mathrm{e_{CB}}^- \quad (2)$$

Fig. 6a illustrates the electron injection process described above with neutral exciplex as a possible intermediate, and Fig. 6b shows the corresponding energy level diagram.

As we mentioned Section 2.2, in N3/ZnO the N3 dye molecules undergo aggregation by forming a complex with Zn^{2+} ions when the concentration of N3 is relatively high on the ZnO surface [10,15]. We have measured the transient absorption spectra in the visible and near-IR range as a function of dye concentration by femtosecond spectroscopy. It was found that the dynamics of the near-IR band did not depend on the amount of N3 loading. This indicates that high loading simply increases the amount of dyes inefficient for electron injection but does not change the rate of injection from active dyes, which are probably adsorbed on the surface in a monomeric form.

We now compare our results on N3/ZnO with well-known results on N3/TiO_2. Ultrafast (<100 fs) electron transfer from photoexcited Ru-complexes or aromatic dye molecules anchored on the TiO_2 surface into the TiO_2 conduction band is a general phenomenon, if the excited molecule has a large enough redox potential and is in close contact with the surface. Recently, it has been reported that electron transfer from photoexcited alizarin to TiO_2 occurs in 6 fs [31]. One of the reasons for such ultrafast electron transfer is considered to be a large number of electron acceptor states in the conduction band. Ellingson and co-workers [18] observed

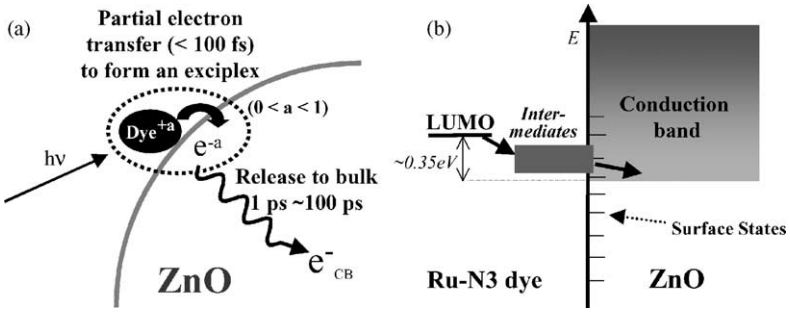

Fig. 6. Scheme to represent the electron injection process in Ru-N3 dye adsorbed on a ZnO nanocrystalline film. (a) Electron transfer partially occurs from photoexcited N3 to the surface state of ZnO to form the intermediate state, which subsequently relaxes to generate the conductive electrons. (b) The corresponding energy diagram. The LUMO of N3 is located 0.35 eV higher than the bottom of the conduction band. Since the energy level of the intermediate is unclear, it is expressed with a thick line. See text for details.

a fast rise (∼50 fs) of strong mid-IR absorption at around 5 μm. In the case of N3/TiO_2, it is concluded that conductive electrons are generated immediately after excitation. Since the density of states of ZnO conduction band is lower by a factor of about 190 than that of TiO_2, slower electron transfer to the conduction band is expected. Our results show that in the case of electron transfer into ZnO, the localized surface states accept electrons to form an intermediate state in the course of electron transfer from the adsorbate to the bulk conduction band.

In conclusion, we have shown that electron transfer from excited molecules to semiconductor occurs stepwise via the intermediate on the surface. The origin of the surface intermediate is at present considered as exciplex due to the interaction between the photoexcited dye and some kind of surface state. So far, attention has been paid to the absorption of dye molecules or conduction band electrons by probing absorption at visible or mid-IR wavelengths, respectively. We have shown that probing absorption in the near-IR range is very powerful in investigating the electron transfer mechanism, especially clarifying how metal oxide nanoparticles accept electrons from photoexcited dye molecules on the surface.

2.4. Efficiency of electron injection

As we mentioned in Section 2.3, the rate of electron injection is very fast. This suggests that the efficiency of electron injection is very high. However, fast injection dynamics does not necessarily lead to a high efficiency of electron injection. This is because, in some cases, inactive dyes, which are not effective for electron injection exist on the surface [8]. To evaluate the electron injection efficiency directly, we have used nano-second transient absorption spectroscopy [8–10]. The absolute value of the efficiency of electron injection can be evaluated from quantitative analysis of transient absorption data. In reality, this is not easy because the estimation of the absorption coefficient of conducting electrons or of oxidized forms of sensitizer dyes is difficult. In Section 2.4.1, our recent attempt for this estimation is described [32]. The estimation of the relative efficiency of electron injection is much easy because it can be evaluated from the apparent absorbance changes of conducting electrons or of oxidized forms of sensitizer dyes, when all measurements are made under the same optical geometry. We have evaluated the efficiency as a function of the free energy change for the electron injection (Section 2.4.3).

2.4.1. Absolute value of efficiency of electron injection in NKX2311/ZnO

We have estimated the absolute value of the efficiency of electron injection in NKX2311/ZnO. For this purpose, the molar absorption coefficient of the oxidized form of NKX2311 must be determined in solution. Upon photoexcitation, an electron transfer reaction from an excited NKX2311 molecule to an electron acceptor occurs and the oxidized form of NKX2311 and the reduced form of the acceptor can be detected. We used methyl viologen trihydrate (MV^{2+}) as an acceptor.

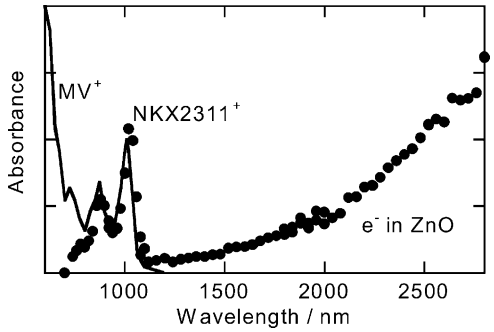

Fig. 7. Transient absorption spectra of: (a) the BQ and (b) the MV^{2+} solutions and of NKX-2311/ZnO.

Fig. 7 shows the transient absorption spectra obtained at 100 ns after 532 nm laser excitation of the NKX2311/MV^{2+} (0.10 M) in CD_3OD. Three absorption bands were observed at 605, 875 and 1010 nm. The peak at 605 nm is assigned to the absorption band of reduced form of MV^{2+} and, therefore, the peaks at 875 and 1010 nm can be assigned to the absorption band of the oxidized form of NKX-2311. By using the value of the molar absorption coefficient of the reduced form of MV^{2+} (12,000 $dm^3\,mol^{-1}\,cm^{-1}$ [33]), the molar absorption coefficient of the oxidized form of NKX2311 can be determined as 6,000 $dm^3\,mol^{-1}\,cm^{-1}$.

Fig. 7 also shows the transient absorption spectrum after 532 nm excitation of NKX2311/ZnO film. The absorption band with peaks at around 880 and 1020 nm are observed, which can be assigned to NKX-2311^+. Absorbance change (ΔA) at time zero of NKX2311^+ monitored at 1020 nm is proportional to laser intensity (I_{ex}). From the absorbance change, the concentration of NKX2311^+ can be estimated and the absolute value of electron injection efficiency from excited NKX2311 into ZnO film was determined as 0.8 ± 0.1.

2.4.2. Effect of aggregation on electron injection efficiency

As we mentioned in Section 2.1.2, N3 dyes form aggregates with Zn^{2+} ions during the preparation of sample specimen. Concerning the effect of the aggregation on the performance of dye-sensitized solar cells, the IPCE dramatically decreases with increasing immersion time of ZnO substrates in N3 dye solution [15]. This implies that the electron injection efficiency is hindered by the formation of the aggregate (N3-Zn^{2+}), although no direct experimental evidence has been reported.

The electron injection efficiency from excited (N3-Zn^{2+}) to ZnO can be evaluated by observing its fluorescence lifetime. The lifetime is found to be 42 ± 3 ns in the synthesized (N3-Zn^{2+}) film and 38 ± 3 ns in (N3-Zn^{2+}) aggregate on the conc. N3/ZnO film at 532 nm light excitation. This clearly shows that, at least part of excited (N3-Zn^{2+}) aggregate do not inject electrons to ZnO in the conc. N3/ZnO film. This

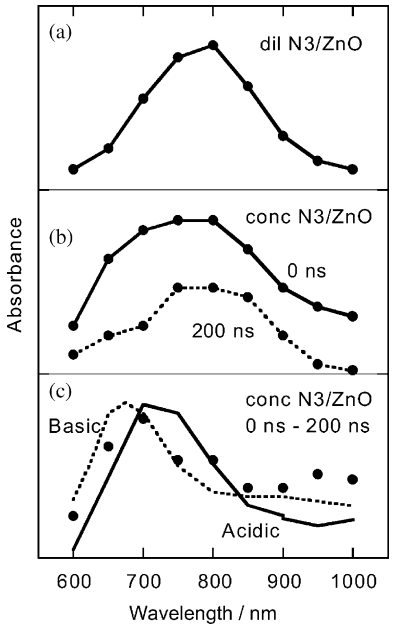

Fig. 8. Transient absorption spectra of dil. N3/ZnO recorded: (a) immediately (at 0 ns) after excitation and (b) at conc. N3/ZnO at 0 ns and at 200 ns. The normalized spectrum of the fast component (0 ns–200 ns) is also shown in (c) (closed circles) together with those of acidic and basic solutions of N3.

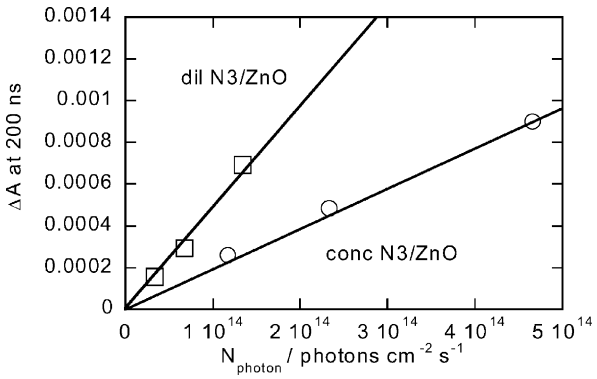

Fig. 9. Absorbance changes at 200 ns after the excitation, probed at 825 nm, as a function of the number of absorbed photons for dil. and conc. N3/ZnO. The slope of the straight line gives the relative efficiency of electron injection from excited sensitizer dyes to ZnO films.

can be explained by the observation made with a scanning electron microscope (SEM) [10] that excited N3 dyes in (N3-Zn^{2+}) are separated away from the surface of the ZnO film by the formation of the micro meter-sized crystals.

The fluorescence lifetime measurement described above clearly shows that some of the aggregates do not inject electrons. However, in the conc. N3/ZnO films, the monomers of N3 dye adsorbed on the surface may inject electrons to the ZnO films. In addition, the electron injection from the aggregates attached directly to the ZnO surface may also be possible. Thus, it is important to estimate the efficiency of the electron injection to compare it with the IPCE of N3/ZnO solar cells.

Fig. 8a shows the transient absorption spectrum of the dil. N3/ZnO film observed immediately after excitation (0 ns). The absorption band with a peak around 800 nm is observed, which can be assigned to oxidized N3 [27]. The oxidized form of N3 in dil. N3/ZnO rises very fast and does not decay up to 200 ns (Fig. 8a). This indicates that the electron injection occurs immediately after excitation and that the recombination is very slow, which is consistent with previous studies [34].

Fig. 8b shows the transient absorption spectra of the conc. N3/ZnO film observed at 0 ns and at 200 ns after excitation. The time profile of the absorption observed at 825 nm can be reproduced using two components, i.e., a decay component with lifetime of $\tau_{fast} = 36 \pm 5$ ns and the time-independent background. The fast decay component can be assigned to the excited (N3-Zn^{2+}) aggregate from the similarity of its lifetime to the fluorescence lifetime of (N3-Zn^{2+}) aggregate on conc. N3/ZnO (38 ns). At 200 ns the absorption due to excited (N3-Zn^{2+}) aggregate decays completely and only the absorption band with the peak around 800 nm remains.

The spectrum of dil. N3/ZnO at 0 ns is very similar to that of conc. N3/ZnO at 200 ns. The spectra of fluorescence and transient absorption of (N3-Zn^{2+}) are different from those of the monomeric form of N3 as seen from Figs. 3 and 8c, respectively. This suggests that the electronic state of N3 is perturbed by the aggregation. The 200 ns spectrum of conc. N3/ZnO can be assigned to the oxidized form of the monomeric N3, namely, the electron transfer occurs mainly from excited monomeric N3. This implies that the aggregates are formed on the surface covered with the monomeric N3.

The spectrum of the fast decay component in Fig. 8b can be obtained by subtracting the spectrum at 200 ns from that at 0 ns and is shown in Fig. 8c. It is obvious that the spectrum of the fast component is different from that of oxidized N3 dye, suggesting that the fast decay is not due to charge recombination. In figure, the transient absorption spectra of N3 in acidic and basic solutions are also shown for comparison. The spectrum of the fast component is slightly different from those of N3 in acidic and basic solutions. This indicates that the transient absorption spectrum of N3 is sensitive to the ions attached to the carboxyl groups.

In both dil. and conc. N3/ZnO, the electron injection occurs mainly from monomeric form of N3, as we discussed above. Thus, the relative efficiency of the electron injection can be evaluated from the absorbance due to the oxidized form of N3. For conc. N3/ZnO, the absorption of the excited (N3-Zn^{2+}) aggregate and of the oxidized N3 dye overlap with each other. The absorption of the excited (N3-Zn^{2+}) decays completely at 200 ns and that of the oxidized N3 dye does not. Therefore, the relative efficiency can be evaluated from the absorbance change at 200 ns.

Fig. 9 shows the absorption A_{ox} of the oxidized N3 dye at 825 nm as a function of the number N_{photon} of absorbed photons evaluated as a product of the exciting light intensity I_{ex} and the light harvesting efficiency, $1 - T$, where T is the transmittance of the sample specimen at the excitation

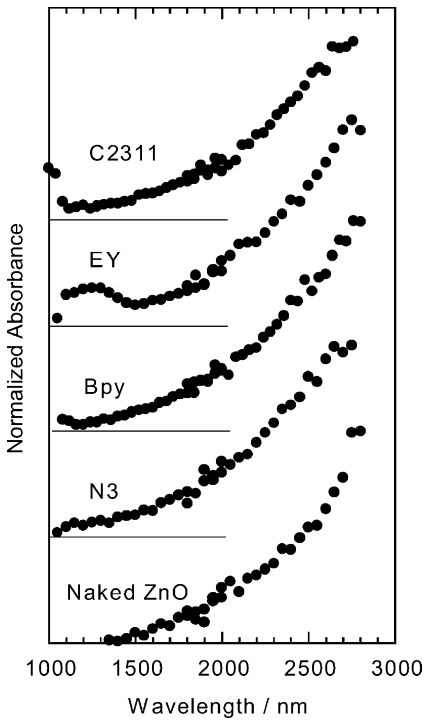

Fig. 10. Transient absorption spectra of naked ZnO film (bottom) and ZnO film sensitized by N3, Bpy, EY, C2311, and C2195.

wavelength (532 nm). It has been pointed out that the decay becomes faster with increasing excitation intensity [23,24]. Thus, we measured the transient absorption under weak excitation conditions (I_{ex} = 0.04–0.14 mJ cm^{-2}). Under this condition, the decay profile is not sensitive to the exciting light intensity. As seen from Fig. 9, A_{ox} is proportional to N_{photon} and the slope of the line gives the relative efficiency of electron injection (see Eq. (1)). The electron injection efficiency is decreased by the aggregation, namely, the electron injection efficiency of conc. N3/ZnO is about one third of that of dil. N3/ZnO.

2.4.3. *Effect of the free energy change on the efficiency of electron injection*

The free energy change ΔG for electron injection is one of the most important factors to determine the electron transfer process. For dye-sensitized nanocrystalline semiconductor systems the relationship between the electron injection process and the free energy change has not been discussed in detail.

2.4.3.1. Relative efficiency of electron injection for various dyes adsorbed on ZnO surface. Conducting electrons in nanocrystalline ZnO film show a broad spectrum in the near IR wavelength range (Fig. 10). The absorbance change is proportional to the number of electrons injected by light irradiation. Thus, the relative efficiencies of electron injection can be evaluated, if all measurements are carried out under the same optical geometry and the correction is

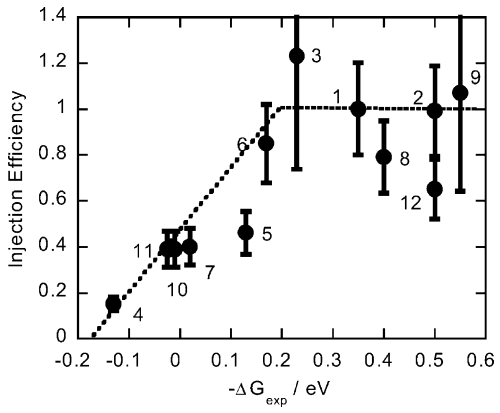

Fig. 11. Relative efficiencies of the electron injection as a function of $-\Delta G_{exp}$. Numbers in the figure represent the compounds listed in Fig. 2.

made for the number of absorbed photons. We already estimated the absolute value of the efficiency in NKX2311/ZnO (Section 2.4.1), so that the absolute values of the efficiencies of other systems can be estimated.

The free energy change ΔG_{exp} obtained experimentally can be expressed as:

$$-\Delta G_{exp} = eE_{CB}{}^{ZnO} - eE_{OX}{}^{dye*} \quad (3)$$

where $E_{CB}{}^{ZnO}$ is the energy of the bottom of the conduction band of ZnO and $E_{OX}{}^{dye*}$ the oxidation potential of the sensitizer dye in the excited state. It is reported that $E_{CB}{}^{ZnO}$ depends on pH of the solvent, $E_{CB}{}^{ZnO} = -0.2$ V at pH = 1 and -0.4 V at pH = 4.8 versus NHE [2]. We assume that the effective pH of dried specimen is pH = 7 and estimate $E_{CB}{}^{ZnO} = -0.5$ V at pH = 7 by extrapolation of the reported values.

Recently, electron injection from unrelaxed states of excited dyes has been observed in N3/TiO_2 [29], bpy/SnO_2, [35] and N3/SnO_2 [36]. However, electron injection in the picosecond time range is dominant for N3/ZnO as we demonstrated in Section 2.3. Thus, we consider that the electron injection occurs from the relaxed excited state of the sensitizer dyes. In this case, $E_{OX}{}^{dye*}$ can be expressed as

$$E_{OX}{}^{dye*} = eE_{OX}{}^{dye} - E_{0-0} \quad (4)$$

where E_{0-0} is the energy of the relaxed excited state, which can be obtained from the onset energy of the ground state absorption spectrum. In the case of Ru-complex, the rate of intersystem crossing from the singlet excited state to the triplet excited state is known to be very fast [30], and is comparable to the relaxation rate from the higher excited states. Therefore, the onset energy of the emission from the triplet state is used as E_{0-0}. In Table 1 of ref. [9], the oxidation potentials (versus NHE) and the E_{0-0} of sensitizer dyes studied are listed.

Fig. 11 show the efficiencies Φ_{inj} of electron injection as a function of $-\Delta G_{exp}$. We estimated the absolute value of the efficiency of electron injection in NKX2311/ZnO (Section 2.4.1). By using this value relative efficiencies

obtained from absorbance of conducting electron can be converted into absolute efficiencies. As shown in Fig. 11, the relative efficiency Φ_{inj} increases with increasing $-\Delta G_{exp}$ in the neighborhood of $-\Delta G_{exp} = 0$ eV and is constant at negative ΔG_{exp}.

2.4.3.2. Model of the electron injection from excited dyes to nanocrystalline films. We have developed a model of electron injection from excited sensitizer dyes to nanocrystalline film to explain the ΔG dependence of the efficiency. For electron transfer reactions in solution, many theories, including the Marcus theory have been proposed and they were successfully applied to many real systems. In the present system, i.e., in dye-sensitized nanocrystalline semiconductor film dried in air, the conditions for electron transfer reactions are different from those in solution. In the present system, the acceptor level (conduction band of the semiconductor) is a continuum and no solvation process is induced by solvent reorganization.

Sakata and coworkers studied the electron transfer process in dye-adsorbed semiconductor powder crystal by picosecond time-resolved fluorescence spectroscopy [37] and proposed a model of the electron injection process from excited dyes to the conduction band of the semiconductor [38]. They assumed an ideal system of no reorganization energy and a parabolic conduction band. Although multi-exponential decay kinetics of fluorescence was observed, they evaluated the electron injection rate constant from the fastest decay component which was the main decay component. They successfully explained the observed dependence of the injection rate on the free energy change on the basis of the proposed model. In dye-sensitized nanocrystalline semiconductor systems multi-exponential kinetics of electron injection has also been observed for TiO_2 [27,29], ZnO [11,20,21] and SnO_2 [21,35,36] by ultra-fast spectroscopy. The deviation from exponential kinetics is more significant in these systems than in powder crystals. This may be due to a morphology difference between nanocrystalline films and powder crystals. This suggests that the model proposed by Sakata et al. [38] may not be directly applicable to the present systems. We have to take into account the energy distribution originating from the site heterogeneity explicitly. Tachibana et al. presented the model with the site heterogeneity to explain the kinetics of electron injection [39]. However, this model cannot be applied directly to discuss the relationship between the efficiency of the injection and ΔG.

The energy distribution may be due to morphology of the surface. It is reported that the energy level of the conduction band edge depends on the crystal face. The conduction band edge of anatase (1 0 1) face of TiO_2 is shifted negatively by 0.2 V relative to that of rutile (0 0 1) face [40]. For nanocrystalline films, many crystal faces as well as crystal structures exist at the surfaces. Therefore, ΔG of the electron injection is different from site to site. Recently, Lu and Xie studied microscopically electron transfer reactions by using single molecule fluorescence technique for organic dyes on ITO films [41]. According to their results, each molecule shows single exponential decay but the lifetimes are different from site to site. On the other hand, multi-exponential decay was observed in conventional fluorescence decay measurements. This indicates that the site heterogeneity is essential to explain multi-exponential kinetics of the electron injection process at interfaces.

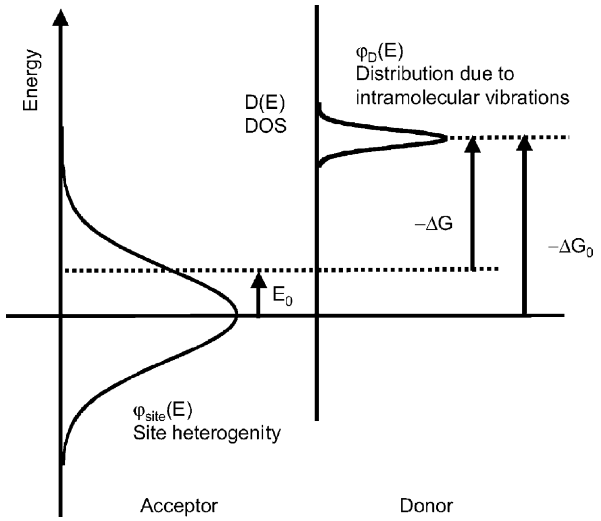

Fig. 12. Energy level diagram for the model of electron injection at semiconductor surface. $\varphi_D(E)$ and $\varphi_{site}(E)$ represent the distribution due to intramolecular vibration and the site heterogeneity, respectively. $D(E)$ represents the density of state of ideal crystal. ΔG is the free energy change of the electron injection at a given site and ΔG_0 is the peak energy of the distribution of the free energy change due to site heterogeneity.

The rate constant k_{ET} of the electron injection can be expressed generally as [42]:

$$k_{ET} = \frac{2\pi}{\hbar} J^2 \int_{-\infty}^{+\infty} \Psi_i(E)\Psi_f(E)dE \quad (5)$$

where J is the transfer integral (the electronic coupling matrix element for the electron transfer reaction), $\Psi_i(E)$ and $\Psi_f(E)$ are the electron detachment spectrum and the electron attachment spectra, respectively. The transfer integral decreases exponentially with increasing distance d between the donor and the acceptor as:

$$J = J_0 \exp(-\beta d) \quad (6)$$

where J_0 is the value at $d = 0$ and β a constant and estimated as $\beta = 1\,\text{Å}^{-1}$ [43]. In the present system, the donor molecule is attached tightly to the semiconductor surface through a carboxyl group as an anchor. Thus, the distance between the donor and the acceptor is constant. Therefore, J is also constant. Fig. 12 illustrates the energy level diagram of the donor and the acceptor for the electron injection process at the interface in the presence of the site heterogeneity. The energy distribution $\varphi_D(E)$ of the excited sensitizer dye originates from the intramolecular vibrations of the sensitizer dye. In the present system, there is no solvent molecule. Therefore the energy distribution originating from the surrounding solvent molecules can be neglected. The electron

injection occurs from the donor state to the conduction band of the ZnO film. The density of states (DOS) of the conduction band is represented by $D(E)$ and the bottom of the conduction band has a distribution originating from the site heterogeneity $\varphi_{site}(E_0)$. These energy distributions can be expressed as:

$$\varphi_D(E) = \frac{1}{(4\pi k_B T\lambda_v)^{1/2}} \exp\left[-\frac{(E + \Delta G_0 + \lambda_v)^2}{4k_B T\lambda_v}\right], \quad (7)$$

$$D(E) = \frac{1}{2\pi^2}\left(\frac{2m}{\hbar^2}\right)^{3/2}\sqrt{E - E_0}, \quad (8)$$

$$\varphi_{site}(E_0) = \frac{1}{(2\pi\sigma_{site}^2)^{1/2}} \exp\left[-\frac{E_0^2}{2\sigma_{site}^2}\right], \quad (9)$$

where λ_v is the reorganization energy due to the intramolecular vibrations of the sensitizer dyes, m the effective mass of the electron in the semiconductor, and σ_{site} the parameter for the site heterogeneity. The free energy change ΔG of the electron injection can be defined as the energy difference between the bottom of the conduction band and the energy of an excited sensitizer dye. This energy difference changes from site to site. ΔG_0 is the peak energy of the distribution of the free energy change due to the site heterogeneity. Thus, ΔG_0 corresponds to the free energy change ΔG_{exp} estimated experimentally (see Eq. (3)).

For the calculation of the rate constant k_{ET} of electron injection at a given site, $\varphi_D(E)$ can be used as the electron detachment spectrum $\Psi_i(E)$ and $D(E)$ can be used as the electron attachment spectrum $\Psi_f(E)$. k_{ET} is the function of E_0 and ΔG_0. In the present system, we assume that the geometrical structure of adsorbed sensitizer dyes on the surface is fixed and the energy distribution $\varphi_{site}(E_0)$ due to the site heterogeneity is frozen. On the other hand, the electron injection occurs after vibrational relaxation. In other words, the energy fluctuation due to intramolecular vibrational motion can be considered to be faster than the electron injection. Under this condition, the kinetics of the electron injection is expressed as the superposition of single exponential kinetics at each site. The survival probability of the electron injection can be expressed as:

$$P(t) = \exp\left[-k_f t\right] \times \int_{-\infty}^{+\infty} \exp[-k_{ET}(E_0, \Delta G_0)t]\,\varphi_{site}(E_0)dE_0. \quad (10)$$

where k_f is the rate constant of fluorescence decay. The efficiency Φ_{inj} of the electron injection can be written as follows:

$$\Phi_{inj}(\Delta G_0) = \int_{-\infty}^{+\infty} \frac{k_{ET}(E_0, \Delta G_0)}{k_f + k_{ET}(E_0, \Delta G_0)}\,\varphi_{site}(E_0)dE_0. \quad (11)$$

The distribution $\varphi_{site}(E_0)$ of the conduction band bottom at different sites is important to explain the multi-exponential kinetics of the electron injection. If the fluctuation in this distribution is much faster than that of the electron injection rate, the survival probability $P(t)$ can be expressed as:

$$P(t) = \exp[(-k_f + k_{ET}(\Delta G_0))t]. \quad (12)$$

$$k_{ET}(\Delta G_0) = \int k_{ET}(E_0, \Delta G_0)\,\varphi_{site}(E_0)dE_0. \quad (13)$$

In this case, the kinetics of electron injection can be fitted by a single exponential function. The efficiency of the electron injection can be expressed simply as:

$$\Phi_{inj}(\Delta G_0) = \frac{k_{ET}(\Delta G_0)}{k_f + k_{ET}(\Delta G_0)}. \quad (14)$$

The conventional relationship described above has been widely used to estimate the injection efficiency. However, this relationship cannot be applied to the system which shows multi-exponential kinetics, such as the electron injection process in nanocrystalline film.

The efficiency of the electron injection as a function of $-\Delta G_0$ can be evaluated using Eq. (11). We assume the reorganization energy due to intramolecular vibrations as $\lambda_v = 0.1$ eV. In order to evaluate the efficiency of electron injection, we assume the rate constant at $-\Delta G = 0.35$ eV to be $k_{ET} = 10^{11}\ s^{-1}$, since it is reported that the injection from N3 occurs within 1–10 ps time range [11,20,21]. For comparison with the experimental data, the value of the rate constant k_f of fluorescence decay of sensitizer dyes is required. However, the rate constant of the fluorescence decay differs from one dye to another, for example, $k_f^{-1} = 2$ ns for C2311 [12] and $k_f^{-1} = 25$ ns for N3 [27]. To obtain the tendency of the dependence of the efficiency on $-\Delta G_0$, we assume $k_f^{-1} = 10$ ns for all dyes considered.

Fig. 13 shows the efficiency calculated using the values $\lambda_v = 0.1$ eV and $\sigma_{site} = 0$, 0.1, 0.2, 0.3 eV by the solid lines and using $\lambda_v = 0.2$ eV and $\sigma_{site} = 0$ eV by the dotted line. In order to compare the experimental data with the model calculation, we assume the relationship; $-\Delta G_0 =$

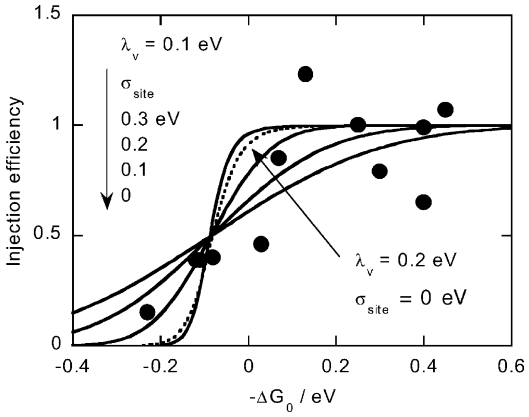

Fig. 13. Relative injection efficiency as a function of $-\Delta G_0$, using the values $\lambda_v = 0.1$ eV, and $\sigma_{site} = 0$, 0.1, 0.2, 0.3 eV (solid line) and $\lambda_v = 0.2$ eV, and $\sigma_{site} = 0$ eV (dotted line). The experimental data are plotted using the relationship; $-\Delta G_0 = \Delta G_{exp} - 0.1$.

$-\Delta G_{exp} - 0.1$ eV. The difference between $-\Delta G_0$ and $-\Delta G_{exp}$ may be due to oversimplification of the method for estimating $-\Delta G_{exp}$. The shape of the injection efficiency seems to be insensitive to λ_v. The efficiency increases steeply with increasing $-\Delta G_0$ in the absence of the site heterogeneity ($\sigma_{site} = 0$ eV), whereas the experimental data increases gradually. This clearly indicates that the $-\Delta G_0$ dependence cannot be explained only by the effect of the reorganization due to intramolecular vibrations. Inclusion of the site heterogeneity is required to explain the tendency of the injection efficiency. The experimental data are scattered between the curve for $\sigma_{site} = 0.1$ eV and that for 0.2 eV. Thus, the most probable value seems to be $\sigma_{site} = 0.15$ eV. The injection efficiency increases gradually with increasing $-\Delta G_0$ between -0.4 and 0.2 eV and above 0.2 eV it tends to saturate. According to our model, the gradual increase of the efficiency around $-\Delta G_0 = 0$ eV reflects the site heterogeneity. Because of the site heterogeneity, even at a fixed value of ΔG_0 some excited molecules have positive $-\Delta G$ values and undergo the injection, while the other have negative $-\Delta G$ values and decay to the ground state.

In the present model, we take into account the site heterogeneity which is induced by the presence of various crystal faces on the surface. If the crystal particles having one crystal face is used as sample, $-\Delta G$ dependence of the injection efficiency should have a steep rise compared with that in nanocrystalline films. However, ZnO particles having well defined crystal face are not available. For AgBr crystal, well-controlled particles have been used in photographic technology. Tani et al. evaluated the relative efficiency of electron injection in AgBr small crystals [44]. Their results are shown in Fig. 14. The efficiency increases more steeply with increasing $-\Delta G$ than in nanocrystalline ZnO systems. This tendency can be represented by Eq. (11) with no site heterogeneity (solid line in Fig. 14). This again shows that the site heterogeneity is a characteristic property in nanocrystalline films.

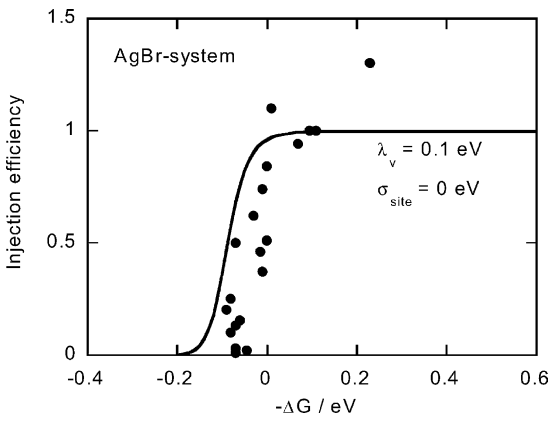

Fig. 14. The efficiency of electron injection in AgBr system. The solid line represents the model calculation using the values of $\lambda_v = 0.1$ eV, and $\sigma_{site} = 0$ eV.

3. Charge recombination

Charge recombination between dye cations and photoinjected electrons occurs non-exponentially over picosecond–millisecond time scales. The wide range of time scales is usually attributed to the trapping of electrons by localized states on the semiconductor surface [23,45–52]. Nanocrystalline materials, possessing a high surface area, have a high density of such intra-band-gap trap states [53]. The distribution of trap energies results in the distribution of electron de-trapping times leading to dispersive transport. Experiments reveal strong sensitivity of the recombination rate to the occupancy of trap levels, which can be controlled by changing the intensity of the light source or the surrounding electrolyte composition, or by applying the external bias [23,46]. Experiments also show that by modifying the dye structure one can switch between electron transport-limited dispersive recombination dynamics and interfacial electron transfer-limited exponential recombination dynamics [54]. This section presents our current understanding of the mechanism of charge recombination in dye-sensitized nanocrystalline TiO_2 films which serves as a basis for our interpretation of available experimental results.

3.1. Mechanism of charge recombination

Fig. 15 illustrates schematically the model of charge recombination. One typically assumes that electrons are rapidly trapped and their concentration in the conduction band is negligible. In TiO_2 trap states are Ti(III) states resulting from the localization of an electron in the Ti 3d orbital in the presence of an electron donating defect (oxygen vacancies, surface binding and intercalation of cations, proton insertion) [55]. The energy distribution of electron trap states $g(\varepsilon)$ is taken to be exponential below the conduction band:

$$g(\varepsilon) = \alpha \exp(-\alpha\varepsilon). \quad (15)$$

Here energy ε is in units of $k_B T$ and the conduction band edge energy is set to zero. Electron transport between trap states is assumed to occur via the multiple trapping

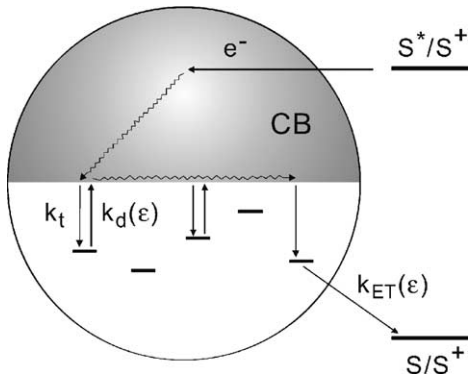

Fig. 15. Model of charge recombination in dye-sensitized semiconductor nanoparticles.

mechanism of conventional semiconductor theory [56]. That is, electrons leave traps by thermal activation to the conduction band and then diffuse in the conduction band until they are trapped again. The de-trapping rate constant is given by:

$$k_d(\varepsilon) = \nu_0 \exp(-\varepsilon), \tag{16}$$

where ν_0 is the attempt-to-escape frequency. After an electron reaches a trap adjacent to the cation, recombination takes place by the electron transfer mechanism with the rate constant k_{ET}. We assume here for simplicity that k_{ET} is neither sensitive to the trap energy nor to its separation from the cation.

Diffusion in the conduction band of TiO_2 is generally believed to be due to small polaron hopping with the electron moving between Ti 3d states that are relatively localized on Ti ions [55]. Defect-induced trap states are similar in nature but more strongly localized and expected to be mainly on the surface of the nanoparticles. No macroscopic electric fields across the sample are assumed because of the screening effect of the electrolyte [53]. Competition of diffusion in the conduction band with trapping gives rise to a distribution of distance an electron can travel between sequential trap states. We can model this distribution by considering diffusive motion of the electron within a spherical nanoparticle of radius R with partially absorbing boundary condition:

$$\frac{\partial}{\partial t}\rho(\boldsymbol{r}, t) = D_{CB}\nabla^2\rho(\boldsymbol{r}, t), \quad 4\pi R^2 D_{CB}\left.\frac{\partial}{\partial r}\rho(\boldsymbol{r}, t)\right|_{r=R} = K_t\,\rho(\boldsymbol{r}, t)|_{r=R}\,. \tag{17}$$

Here, D_{CB} is the diffusion coefficient in the conduction band, $\rho(\boldsymbol{r}, t)$ is the probability density to find the electron at point $\boldsymbol{r}$ within the nanoparticle at time t, and K_t is the trapping rate constant. It is assumed that trapping occurs only at the surface while diffusion occurs in the bulk. Whenever the electron comes to the surface it has a chance to be trapped or to be reflected. K_t is the second-order rate constant. It can be related to the first-order rate constant per trap k_t in a usual way, $k_t = K_t/(NV)$, where N is the number of traps per nanoparticle of volume V. A continuous approach is justified by a typically large N (reportedly [57], several hundred for TiO_2). The distribution $w(\theta, \kappa)$ of angular distance θ between the initial and final position of the electron at the surface can be calculated as an integral of the flux at the surface over time. We obtain:

$$w(\theta, \kappa) = \kappa\sum_{n=0}^{\infty}\frac{n + 1/2}{n + \kappa}P_n(\cos\theta), \tag{18}$$

where $\kappa = K_t/(4\pi D_{CB}R)$ and P_n denotes the Legendre polynomial.

This is, of course, an 'ideal' model but it gives us an idea of how far the electron can travel in the conduction band depending on the ratio of k_t to D_{CB} (see Fig. 16). In the limit of $\kappa \gg 1$, $w(\theta, \kappa)$ is localized around $\theta = 0$, i.e., electron hops only between the nearest-neighboring traps. In the opposite limit of $\kappa \ll 1$, $w(\theta, \kappa)$ approaches a uniform distribution, i.e., electron has an equal chance to be captured by any of the vacant traps within the same nanoparticle. We referred to this situation as the random flight mechanism for lack of a better term [52]. With typical parameters [57,58] ($N = 600$, $R = 10\,\text{nm}$, $D_{CB} = 1.5 \times 10^{-6}\,\text{m}^2\,\text{s}^{-1}$) one can estimate $\kappa \sim 10^{-10}\,k_t$. In accordance with the principle of detailed balance, k_t is equal to the attempt-to-escape frequency ν_0 multiplied by the ratio of the number density of localized trap states to the number density of the conduction band states [56]. Since this ratio is expected to be considerably less than unity and since ν_0 is not expected to exceed the atomic frequency, $\sim 10^{12}\,\text{s}^{-1}$, one may conclude that typically $\kappa \ll 1$, thus corroborating the random flight mechanism.

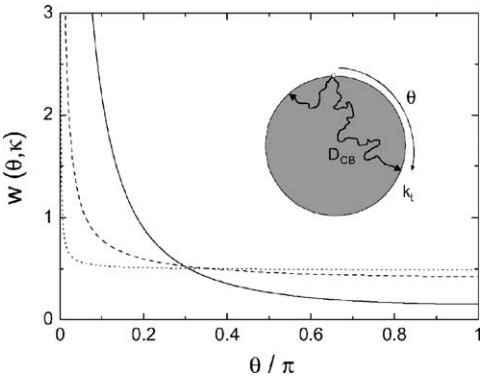

Fig. 16. The distribution of angular distance between surface trap states visited by an electron diffusing in the conduction band of a spherical nanoparticle by successive captures, according to Eq. (18), for different values of the parameter $\kappa = 1$ (solid), 0.1 (dashed), and 0.01 (dotted).

Another argument in favor of the random flight mechanism is that it is analytically tractable. It will be used throughout this section. We will comment, where appropriate, on the possible effects of a more general mechanism. Our consideration will be restricted to recombination within a single nanoparticle. Although electron mobility between nanoparticles is certainly important (the solar cell would not function otherwise), there is indication that under certain experimental conditions recombination could be mainly an intra-particle event: the decay kinetics was observed to become intensity (i.e., concentration) independent as soon as the estimated average number of photoexcited cations per nanoparticle became less than one [23]. In any case, consideration of intra-particle recombination allows us to understand the basic physics of the phenomenon.

3.2. Kinetics of charge recombination

Consider a single electron–cation pair in a TiO_2 nanoparticle. The electron undergoes a series of de-trapping–trapping events from one trap to another within the nanoparticle, while the cation resides at its original position. Each de-trapping event is associated with the waiting time

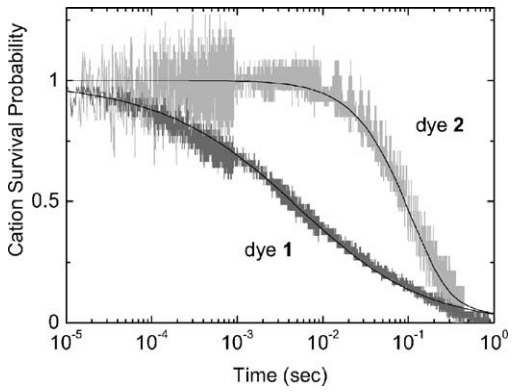

Fig. 17. Normalized transient cation absorption decay data of Clifford et al. [54] (grey lines) for TiO_2 films sensitized with *meso*-5,10,15,20-tetrakis- (4-carboxyphenyl)porphyrin (dye 1) and *meso*-5-(4-carboxyphenyl)-10,15,20-tris-(4-diphenylaminophenyl)porphyrin (dye 2). Solid lines correspond to theory [61] with the following parameters: $\alpha = 0.5$, $p = 0.01$, $\varepsilon_F = 18\,k_BT$, $\nu_0 = 3.2 \times 10^6\,s^{-1}$, and $k_{ET}/\nu_0 = 3.5 \times 10^{-6}$ (dye 2). For dye 1, k_{ET} is assumed to be very high.

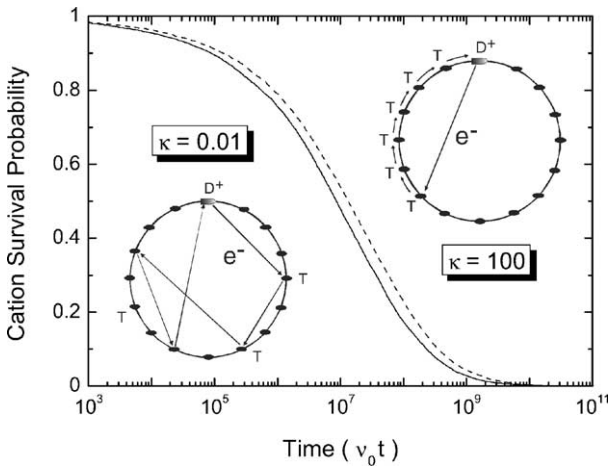

Fig. 18. Numerical simulation results for the cation survival probability within a nanoparticle for different mechanisms of spatial electron transport, as qualified by the jump distribution function of Eq. (18): the random flight ($\kappa = 0.01$, solid line) and the nearest-neighbor random walk ($\kappa = 100$, dashed line). The following parameters were used in simulation: the number of photoinduced cations, $n_0 = 1$, the number of traps, $N = 600$, the Fermi energy, $\varepsilon_F = 20\,k_BT$, and $\alpha = 0.37$. Time is in units of ν_0^{-1}. For the nearest-neighbor mechanism, re-trapping (trapping into the original trap after de-trapping) is not allowed. This is how this mechanism is usually implemented [47]. Effectively, this leads to renormalization of ν_0.

distribution (WTD) function:

$$\psi_d(t) = \int_0^\infty d\varepsilon g(\varepsilon) k_d(\varepsilon) \exp[-k_d(\varepsilon)t]. \quad (19)$$

If the trap energy distribution is given by Eq. (15), the WTD is characterized by the power-law tail, $\psi_d(t) \sim t^{-1-\alpha}$. It is this tail that gives rise to dispersive transport. When the electron reaches a trap site adjacent to the cation (a fraction p of such sites per nanoparticle is assumed), de-trapping competes with recombination. The fate of the electron is then characterized by two WTD functions, the WTD for de-trapping and the WTD for reaction. Let us assume for the time being that recombination is sufficiently fast, i.e., occurs immediately when the adjacent trap is reached. All this is the standard continuous-time random walk (CTRW) formulation where each individual step of the walk is ensemble averaged [59]. Experiment monitors the cation survival probability, $\Phi(t)$. The Laplace transform, $\hat{\Phi}(s) \equiv \int_0^\infty dt \Phi(t) \exp(-st)$, can be calculated using the CTRW formalism as follows:

$$\hat{\Phi}(s) = \frac{1}{s}\left[1 + \frac{p}{(1-p)h(s)}\right]^{-1}, \quad (20)$$

where the hypergeometric function $h(s) = {}_2F_1(1, \alpha, 1+\alpha, -1/s)$ arises due to the functional form of our WTD with the trap energy distribution given by Eq. (15), namely, $\hat{\psi}_d(s) = 1 - h(s)$. Here and henceforth, we set $\nu_0 = 1$, until we compare our results with experiment.

Since $h(s) \sim s^\alpha$ in the limit of $s \to 0$ [60], one can expect the power-law feature in the decay kinetics at long times, i.e., $P(t) \sim t^{-\alpha}$. This behavior is a consequence of the chosen trap energy distribution and the resulting distribution of de-trapping times. Fig. 17 shows the fit of the experimental decay [54] in the transport-limited regime (dye 1) by Eq. (20), which was somewhat modified to account for the presence of dark electrons [61]. However, this modification is insignificant to our discussion because the estimated number density of dark electrons is only about 0.1 per nanoparticle [57]. The concentration of photogenerated electrons in the experiment quoted was low, which justifies the applicability of the geminate recombination theory. Note that the value of ν_0 obtained from the fit suggests that $\kappa \ll 1$ thus supporting the assumed random flight mechanism. This is not a proof, however, because the fraction of adjacent sites (reaction radius) was chosen rather arbitrarily. Smaller p would lead to higher ν_0 values.

Detailed analysis shows [52] that a more general mechanism of electron transport with arbitrary ratio κ of k_t to D_{CB} retains the shape of the decay curve, but the decay becomes a bit slower as κ is increased (see Fig. 18). Roughly speaking, small κ corresponds to our random flight model, while large κ corresponds to Nelson's. Therefore, if Nelson's model is adopted instead of our model, a somewhat larger value of the de-trapping rate is required to reproduce the experimental data. The spatial arrangement of trap sites has also very little effect [48]. We conclude that the observed dispersive recombination kinetics is governed by electron diffusion in energy space through de-trapping–trapping processes rather than conventional diffusion in space. Moreover, it was shown that only a few deep traps are actually responsible for this unusual kinetic behavior [62].

3.2.1. Effect of dye structure

By modifying the structure of the dye one can increase physical separation of the cation from the film surface and/or change the reaction energetics and thus reduce the recombi-

nation rate. Clifford et al. showed [54] that slow kinetics is exponential rather than dispersive, allowing the authors to suggest that it is interfacial electron transfer rather than the electron transport that is the limiting step of reaction. Given dispersive transport, the resultant exponential kinetics is not as trivial as it may seem. If we modify the CTRW model described above to take into account a finite rate k_{ET} of back electron transfer, it turns out that k_{ET} will only modulate the decay but the kinetics will remain dispersive [61]. This puzzle can be resolved by taking Coulomb interaction between an electron and a cation into account. This interaction is certainly not long-ranged because of the screening effect of the surrounding electrolyte. However, it should be strong when the two charges are close. An electron trapped at one of the sites adjacent to the cation will have its activation energy for de-trapping increased by the Coulomb contribution. If we assume that the Coulomb energy is much larger than the usual trap energy, then an electron, once reaching a trap site adjacent to the cation will no longer be de-trapped. Effectively, once an electron reaches a trap site adjacent to the cation, it is no longer de-trapped. This idea can be readily incorporated into the CTRW formulation giving us the result [61]:

$$\hat{\Phi}(s) = \frac{1}{s} - \frac{k_{ET}}{s(s+k_{ET})}\left[1 + \left(\frac{1}{p} - 1\right) h(s)\right]^{-1}. \tag{21}$$

For high values of k_{ET}, Eq. (21) reduces to Eq. (20) and describes transport-controlled dispersive kinetics. However, when k_{ET} is sufficiently small, Eq. (21) predicts an intermediate exponential stage. The decay curves for different k_{ET} converge at long times. The long-time behavior is dispersive and independent of k_{ET}. Let us take another look at Fig. 17. In order to fit the experimental decay for dye 2, we have taken the parameters from the fit for dye 1 and then adjusted k_{ET}. Good agreement suggests that the Coulomb trap mechanism may be correct.

3.2.2. Effect of light intensity

Dispersive recombination kinetics results from the wide distribution of de-trapping times and, therefore, should be very sensitive to the occupancy of the trap states. The effect is nonlinear in concentration, because of a nonlinear relationship between the electron number density and the Fermi energy. This phenomenon manifests itself in the observed dramatic dependence of the recombination rate on the incident light intensity and external bias [23,46].

High intensity of incident light may lead to a situation where the number of electron–cation pairs generated per nanoparticle is more than one. The observed bulk recombination rate is expected to increase for two reasons. Firstly, because the concentration is increased, and secondly, because the effective electron mobility is increased. Some electrons will fill deeper traps thereby increasing the mobility of other electrons. This problem can be approached [52] via the master equation for the probability distribution function of trapped electrons, $f(\varepsilon, t)$:

$$\frac{\partial}{\partial t} f(\varepsilon, t) = -k_d(\varepsilon) f(\varepsilon, t) + \frac{Ng(\varepsilon) - f(\varepsilon, t)}{N} \times \int_0^\infty d\varepsilon k_d(\varepsilon) f(\varepsilon, t), \tag{22}$$

with the initial condition, $f(\varepsilon, 0) = n_0 g(\varepsilon)$. Here, N is the number of traps and n_0 the initial number of photogenerated electrons (also cations) per nanoparticle. The time-dependent number density of electrons is given by $n(t) \equiv \int_0^\infty d\varepsilon f(\varepsilon, t)$, while the survival probability is expressed as $\Phi(t) \equiv n(t)/n_0$. As in the original work, here we assume that the recombination occurs by the same mechanism as the trapping (i.e., via the conduction band) with the only difference that the recombination is irreversible. This is equivalent to the assumption of one reactive trap per cation, $p = 1/N$, if the recombination mechanism is described by electron transfer.

The meaning of Eq. (22) is quite clear: the first term on the right-hand side corresponds to de-trapping. On the other hand, the second term represents the total de-trapping rate multiplied by the density of vacant traps and corresponds to trapping. The solution for the survival probability can be written in the standard form known for bimolecular reactions with equal reactant concentrations, i.e.,

$$\Phi^{-1}(t) = 1 + \frac{n_0}{N}\int_0^t dt'\, k(t'), \tag{23}$$

where the rate coefficient $k(t)$ is given in terms of its Laplace transform, $\hat{k}(s) = h^{-1}(s) - 1$. In usual kinetics (such as in the case of diffusion-limited reactions), $k(t)$ rapidly relaxes to a constant value, so that $P(t)$ behaves as $\sim t^{-1}$. Dispersive transport leads to the result that $P(t)$ decays more slowly, $P(t) \sim t^{-\alpha}$. The following approximation has proven to be sufficiently good:

$$\Phi^{-1}(t) = 1 + \frac{n_0}{N} c t^\alpha, \tag{24}$$

where $c = [\pi\alpha \csc(\pi\alpha)\Gamma(1+\alpha)]^{-1}$ and $\Gamma(x)$ is the gamma function.

Fig. 19 plots experimental transient absorption decay data of Haque et al. [23] for different excitation intensities, in such a way that Eq. (24) gives a straight line. Recombination in an unbiased film appears to obey this simple decay law fairly well over a wide range of times. Although one can further improve the accuracy by incorporating the effect of dark electrons, Eq. (24) is quite sufficient to characterize the general tendency. We should, however, point out that the concentration dependence of the kinetics that is extracted from fitting the data to the random flight model is only in qualitative agreement with the average number of cations per nanoparticle estimated from the experimental excitation intensity. As a reason for this discrepancy one may speculate that photogeneration of cations is a nonlinear function of the excitation intensity when the intensity is high, as it was

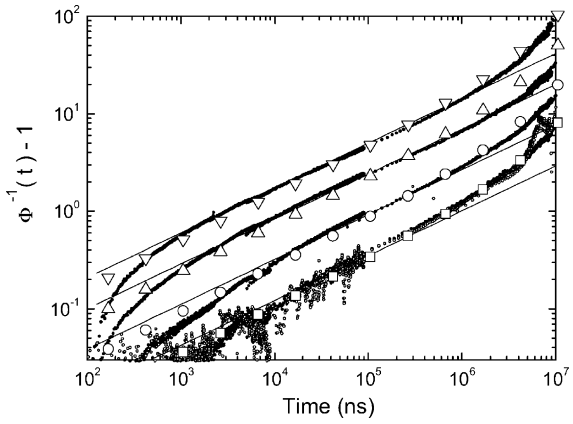

Fig. 19. Transient absorption data of Haque et al. [23] showing the decay of the cation state of $Ru(dcbpy)_2(NCS)_2$ adsorbed on a nanocrystalline TiO_2 film with an ethylene carbonate/propylene carbonate 1:1 electrolyte for different excitation intensities: 0.04 (small open circles), 0.12, 0.6, 3.5, and 6 mJ/cm^2 (full circles, from bottom). Solid straight lines were calculated using Eq. (24) with $\alpha = 0.46$. Large symbols represent a more elaborate theoretical expression [52] for $\varepsilon_F = 17\,k_BT$, $\nu_0 = 1.5 \times 10^9\ s^{-1}$, $\alpha = 0.46$, and $n_0/N = 0.0016$, 0.0042, 0.011, and 0.023 (from bottom).

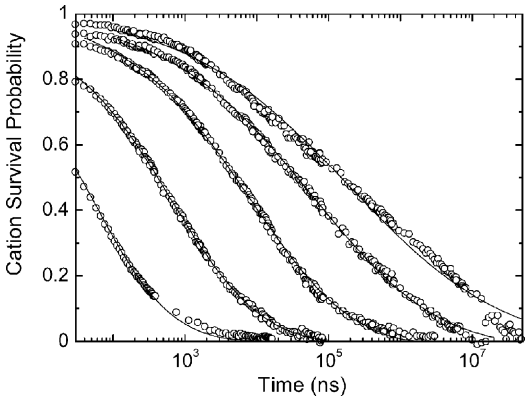

Fig. 20. Transient absorption data of Haque et al. [23] showing the decay of the cation state of $Ru(dcbpy)_2(NCS)_2$ adsorbed on a nanocrystalline TiO_2 electrode with an ethanol/0.1 M tetrabutylammonium triflate electrolyte for different applied potentials: 0, 100, 200, 300, and 400 mV (circles, right to left). Lines were calculated [52] for $n_0/N = 0.0016$ (one cation per nanoparticle) and $\nu_0 = 2.6 \times 10^{11}\ s^{-1}$. The parameters obtained from fitting are: $\alpha = 0.37$, 0.4, 0.47, 0.58, 0.81 and $\varepsilon_F = 25.1$, 21.1, 17.9, 15.5, 13.1 k_BT (right to left).

indeed observed in some experiments. Some deficiency of the model may also be considered.

3.2.3. Effect of applied bias

Applied bias changes the electron Fermi level. The higher this level is, the larger is the number of dark electrons occupying trap states prior to photoexcitation. Dark electrons are in thermal equilibrium. The number density of dark electrons n_d is related to the Fermi energy ε_F as follows:

$$n_d = N\int_0^\infty d\varepsilon \frac{g(\varepsilon)}{1+\exp(\varepsilon_F-\varepsilon)} = h[\exp(-\varepsilon_F)], \qquad (25)$$

in accordance with the Fermi statistics. Approximately, $n_d \sim \exp(-\alpha\varepsilon_F)$. The recombination rate is expected to increase with applied bias for the same two reasons considered in the effect of light intensity, i.e., the increase in electron concentration and the trap filling effect.

We consider a bimolecular reaction where one reactant is in excess and moving (electrons) and the other reactant (cation) is immobile. This is known in chemical kinetics as the target problem [63]. If the concentration of electrons is so low that their mutual interference is negligible, then one can use a standard solution to this problem:

$$\phi(t) = \exp\left(-\frac{n_e}{N}\int_0^t dt' k(t')\right) \cong \exp\left(-\frac{n_e}{N}ct^\alpha\right), \qquad (26)$$

which leads to a stretched exponential decay. Here, $n_e = n_0 + n_d$. Eq. (26) assumes that each trap is characterized by the WTD of Eq. (19), that is, the WTD obtained by averaging over the energy distribution of *all* traps. However, a photogenerated electron (subsequently, any de-trapped electron) can be trapped only into vacant traps. Therefore, a more appropriate approximation for the WTD would be obtained by averaging $k_d(\varepsilon)\exp[-k_d(\varepsilon)t]$ over the distribution of *vacant* traps, i.e., over $g(\varepsilon)$ minus the Fermi distribution. The reaction is expected to be controlled by de-trapping at the Fermi level. When $n_0 \ll n_d$, the total Fermi level in the system will deviate from the dark Fermi level only slightly. Therefore, we can expect that $\Phi(t) \sim \exp[-k_d(\varepsilon_F)t]$. More detailed consideration and solution of the master equation for the probability distribution function of trapped electrons leads to the following approximate expression for the survival probability [52]:

$$\Phi^{-1}(t) = \exp(te^{-\varepsilon_F}) + \frac{n_0}{N}ct^\alpha, \qquad (27)$$

as a natural generalization of Eq. (24). The first term on the right-hand side of Eq. (27) shows the effect of dark electrons, while the second term can be ascribed to photogenerated electrons.

Fig. 20 shows experimental transient absorption decay data of Haque et al. [23] as a function of applied bias and theoretical fit (a somewhat more complicated formula than Eq. (27) was used). Although the random flight model provides a qualitative explanation for the applied bias effect, we have not been able to fit all the data consistently with one set of parameters varying only the number of dark electrons. Nelson et al. [48] achieved certain consistency on the basis of the nearest-neighbor random walk mechanism [47]. However, the value for the attempt-to-escape frequency obtained from the fit was far too high. It is very likely that the intermediate regime of electron spatial diffusion is realized, where there is a certain probability for an electron to travel a certain distance between localized surface traps by diffusion in the conduction band. We should emphasize that all models agree nicely as far as the dependence of the half-time for re-reduction of the dye cation, $t_{50\%}$, on the number of dark electrons is concerned. $t_{50\%}$ is defined by $\Phi(t_{50\%}) = (1/2)\Phi(0)$. The power-law

dependence,

$$t_{50\%} \approx n_d^{-1/\alpha}, \quad (28)$$

observed experimentally by Nelson et al. [48] is corroborated both by Eqs. (26) and (27) for sufficiently large n_d. Recall that $\exp(-\varepsilon_F) \sim n_d^{1/\alpha}$. This coincidence gives extra support to the conclusion that the dominant role in influencing the recombination kinetics is played by the redistribution of electrons among traps of different energy rather than by spatial diffusion.

In concluding this section we would like to comment that so far there is no consensus in the literature regarding the number of traps per nanoparticle. For example, by comparing their transient photocurrent measurements with random walk simulations Van de Lagemaat and Frank [64] have concluded that only one trap per nanoparticle is required to achieve consistency. This looks like a contradiction to our and others' assumption [47,48,52,57] that this number is about several hundred. However, in our opinion there is no contradiction. Results of Van de Lagemaat and Frank only confirm that the conduction band in nanocrystalline TiO_2 films is not continuous through the sample but rather discontinuous at particle boundaries. Hopping through these boundaries controls macroscopic electron transport. In macroscopic electron transport a nanoparticle itself acts as a trap. Consideration of the recombination kinetics, on the other hand, requires details of the intra-particle electron motion (energy redistribution) to be taken into account, where many trap states are involved.

4. Concluding remarks

We have reviewed our recent experimental and theoretical work on the kinetics and mechanism of electron injection and charge recombination in dye-sensitized nanocrystalline semiconductors. In our experimental studies of electron injection, we have used nanocrystalline ZnO films as the semiconductor. In order to reveal the kinetics and mechanism of electron injection we have developed several types of transient absorption spectrometers which enable us to observe the time profiles of the absorption spectra of the oxidized form of dyes and conducting electrons with high sensitivity over a wide wavelength range from near IR to visible and over a wide time range from femtoseconds to submicroseconds. For N3 dye/ZnO system, we have clarified the aggregation of N3 dyes and its effect on electron injection spectroscopically. We have also measured the electron injection process by a femtosecond pump-probe method and shown that a fraction of electron injection occurs via an intermediate state. We have determined the absolute efficiency of electron injection and developed a new theoretical model for electron injection to explain the dependence of the efficiency of electron injection on the free energy change for injection. Concerning charge recombination we have developed a consistent theoretical model which explains not only the observed highly dispersive kinetics of charge recombination but also the effects of the light intensity, the applied bias and the dye structure on the kinetics.

Acknowledgements

We acknowledge Drs. K. Hara, H. Horiuchi, M. Yanagida and S. Suga for their help in the experiments and Drs. H. Sugihara, S. Murata, Y. Tachibana, and K. Seki for useful discussions. This work was supported by the COE development program of the Ministry of Education, Culture, Sports, Science and Technology (MEXT) of Japan.

References

[1] M.K. Nazeeruddin, A. Kay, I. Rodicio, R. Humphry-Baker, E. Muller, P. Liska, N. Vlachopoulos, M. Grätzel, J. Am. Chem. Soc. 115 (1993) 6382.
[2] K. Kalyanasundaram, M. Grätzel, Coord. Chem. Rev. 77 (1998) 347.
[3] G. Redmond, D. Fitzmaurice, M. Grätzel, Chem. Mater. 6 (1994) 686.
[4] H. Resmo, K. Keis, H. Lindström, S. Södergren, A. Solbrand, A. Hagfeldt, S.-E. Lindquist, J. Phys. Chem. B 101 (1997) 2598.
[5] I. Bedja, P.V. Kamat, X. Hua, A.G. Lappin, S. Hotchandani, Langmuir 13 (1997) 2398.
[6] K. Sayama, M. Sugino, H. Sugihara, Y. Abe, H. Arakawa, Chem. Lett. (1998) 753.
[7] K. Hara, T. Horiguchi, T. Kinoshita, K. Sayama, H. Sugihara, H. Arakawa, Chem. Lett. (2000) 316.
[8] K. Hara, H. Horiuchi, R. Katoh, L.P. Singh, H. Sugihara, K. Sayama, S. Murata, M. Tachiya, H. Arakawa, J. Phys. Chem. B 106 (2002) 374.
[9] R. Katoh, A. Furube, K. Hara, S. Murata, H. Sugihara, H. Arakawa, M. Tachiya, J. Phys. Chem. B 106 (2002) 12957.
[10] H. Horiuchi, R. Katoh, K. Hara, M. Yanagida, S. Murata, H. Sugihara, H. Arakawa, M. Tachiya, J. Chem. Phys. B 107 (2003) 2570.
[11] A. Furube, R. Katoh, K. Hara, S. Murata, H. Arakawa, M. Tachiya, J. Phys. Chem. B 107 (2003) 4162.
[12] K. Hara, T. Sato, R. Katoh, A. Furube, Y. Ohga, A. Shinpo, S. Suga, K. Sayama, H. Sugihara, H. Arakawa, J. Phys. Chem. B 107 (2003) 597.
[13] R. Baumeler, P. Rys, H. Zollinger, Helv. Chim. Acta 56 (1973) 2450.
[14] K.H. Hauffe, Photogr. Sci. Eng. 20 (1976) 124.
[15] K. Keis, J. Lindgren, S.E. Lindquist, A. Hagfeldt, Langmuir 16 (2000) 4688.
[16] M.K. Nazeeruddin, S.M. Zakeeruddin, R. Humphry-Baker, M. Jirousek, P. Liska, N. Vlachopoulos, V. Shklover, C.H. Fisher, M. Grätzel, Inorg. Chem. 38 (1999) 6298.
[17] G. Benkö, M. Hilgendorff, A.P. Yartsev, V. Sundström, J. Phys. Chem. B 105 (2001) 967.
[18] J.B. Asbury, R.J. Ellingson, H.N. Ghosh, S. Ferrere, A.J. Nozik, T. Lian, J. Phys. Chem. B 103 (1999) 3110.
[19] (a) J.B. Asbury, Y. Wang, T. Lian, J. Phys. Chem. B 103 (1999) 6643;
(b) J.B. Asbury, E. Hao, Y. Wang, H.N. Ghosh, T. Lian, J. Phys. Chem. B 105 (2001) 4545.
[20] N.A. Anderson, X. Ai, T. Lian, J. Phys. Chem. B 107 (2003) 14414.
[21] A. Yamakata, T. Ishibashi, H. Onishi, Chem. Phys. Lett. 333 (2001) 271.
[22] H. van't Spijker, B. O'Regan, A. Goossens, J. Phys. Chem. B 105 (2001) 7220.

[23] S.A. Haque, Y. Tachibana, R.L. Willis, J.E. Moser, M. Grätzel, D.R. Klug, J.R. Durrant, J. Phys. Chem. B 104 (2000) 538.
[24] T.A. Heimer, E.J. Heilweil, C.A. Bignozzi, G.J. Meyer, J. Phys. Chem. A 104 (2000) 4256.
[25] R. Katoh, S. Sinha, S. Murata, M. Tachiya, J. Photochem. Photobiol. A: Chem. 145 (2001) 23.
[26] R. Katoh, S. Sinha, S. Murata, M. Tachiya, Chem. Phys. Lett. 352 (2002) 234.
[27] Y. Tachibana, J.E. Moser, M. Grätzel, D.R. Klug, J.R. Durrant, J. Phys. Chem. 100 (1996) 20056.
[28] J.I. Pankove, Optical Processes in Semiconductor, Dover, New York, 1975.
[29] G. Benkö, J. Kallioinen, J.E.I. Korppi-Tommola, A.P. Yartsev, V. Sundström, J. Am. Chem. Soc. 124 (2002) 489.
[30] A.C. Bhasikuttan, M. Suzuki, S. Nakashima, T. Okada, J. Am. Chem. Soc. 124 (2002) 8398.
[31] R. Huber, J.E. Moser, M. Grätzel, J. Wachtveitl, J. Phys. Chem. B 106 (2002) 6494.
[32] T. Yoshihara, R. Katoh, A. Furube, M. Murai, T. Tamaki, K. Hara, S. Murata, H. Arakawa, M. Tachiya, J. Phys. Chem. B 108 (2004) 2643.
[33] D. Meisel, W.A. Mulac, M.S. Matheson, J. Phys. Chem. 85 (1981) 179.
[34] R.L. Willis, C. Olson, B. O'Regan, T. Lutz, J. Nelson, J.R. Durrant, J. Phys. Chem. B 106 (2002) 7605.
[35] S. Iwai, K. Hara, S. Murata, R. Katoh, H. Sugihara, H. Arakawa, J. Chem. Phys. 113 (2000) 3366.
[36] G. Benkö, P. Myllyperkiö, J. Pan, A.P. Yartsev, V. Sundström, J. Am. Chem. Soc. 105 (2002) 1118.
[37] K. Hashimoto, M. Hiramoto, A.B.P. Lever, T. Sakata, J. Phys. Chem. 92 (1988) 1016.
[38] T. Sakata, K. Hashimoto, M. Hiramoto, J. Phys. Chem. 94 (1990) 3040.
[39] Y. Tachibana, I.V. Rubtsov, I. Montanari, K. Yoshihara, D.R. Klug, J.R. Durrant, J. Photochem. Photobiol. A Chem. 142 (2001) 215.
[40] L. Kavan, M. Grätzel, S.E. Gilbert, C. Klemenz, H.J. Scheel, J. Am. Chem. Soc. 118 (1996) 6716.
[41] H.P. Lu, X.S. Xie, Z. Phys. Chem. 212 (1999) 59.
[42] M. Tachiya, Radiat. Phys. Chem. 17 (1981) 447.
[43] S. Murata, S.Y. Matsuzaki, M. Tachiya, J. Phys. Chem. 99 (1995) 5354.
[44] T. Tani, T. Suzumoto, K. Ohzeki, J. Phys. Chem. 94 (1990) 1298.
[45] S.Y. Huang, G. Schlichthörl, A.J. Nozik, M. Grätzel, A.J. Frank, J. Phys. Chem. B 101 (1997) 2576.
[46] S.A. Haque, Y. Tachibana, D.R. Klug, J.R. Durrant, J. Phys. Chem. B 102 (1998) 1745.
[47] J. Nelson, Phys. Rev. B 59 (1999) 15374.
[48] J. Nelson, S.A. Haque, D.R. Klug, J.R. Durrant, Phys. Rev. B 63 (2001) 205321.
[49] G.M. Hasselmann, G.J. Meyer, J. Phys. Chem. B 103 (1999) 7671.
[50] J. Van de Lagemaat, N.-G. Park, A.J. Frank, J. Phys. Chem. B 104 (2000) 2044.
[51] C. Bauer, G. Boschloo, E. Mukhtar, A. Hagfeldt, J. Phys. Chem. B 105 (2001) 5585.
[52] A.V. Barzykin, M. Tachiya, J. Phys. Chem. B 106 (2002) 4356.
[53] A. Hagfeldt, M. Grätzel, Chem. Rev. 95 (1995) 49.
[54] J.N. Clifford, G. Yahioglu, L.R. Milgrom, J.R. Durrant, Chem. Commun. (2002) 1260.
[55] P.A. Cox, Transition Metal Oxides, Oxford University Press, Oxford, 1992.
[56] F.W. Schmidlin, Phys. Rev. B 16 (1977) 2362.
[57] G. Rothenberger, D. Fitzmaurice, M. Grätzel, J. Phys. Chem. 96 (1992) 5983.
[58] B. Poumellec, J.F. Marucco, F. Lagnel, Phys. Status Solidi A 89 (1985) 375.
[59] G.H. Weiss, Aspects and Applications of the Random Walk, North-Holland, Amsterdam, 1994.
[60] M. Abramowitz, I.A. Stegun, Handbook of Mathematical Functions, Dover, New York, 1970.
[61] A.V. Barzykin, M. Tachiya, Book of Abstracts of 21st International Conference on Photochemistry, Nara, Japan, 26–31 July 2003, p. 334; J. Phys. chem B, in press.
[62] J.A. Anta, J. Nelson, N. Quirke, Phys. Rev. B 65 (2002) 125324.
[63] G. Zumofen, A. Blumen, J. Klafter, J. Chem. Phys. 82 (1985) 3198.
[64] J. Van de Lagemaat, A.J. Frank, J. Phys. Chem. B 105 (2001) 11194.